BMC Microbiology

https://doi.org/10.1186/s12866-025-04564-6

Article in Press

Iron bioremediation by utilizing biochar-bacterial composites

Received: 26 September 2025

Accepted: 17 November 2025

Published online: 16 December 2025

Cite this article as: Bahuguna M., Bhandari G., Joshi N. *et al.* Iron bioremediation by utilizing biochar-bacterial composites. *BMC Microbiol* (2025). https://doi.org/10.1186/s12866-025-04564-6

Mayank Bahuguna, Geeta Bhandari, Nupur Joshi, Prashant Singh, Sanjay Gupta, Saurabh Gangola & Shshank Chaube

Iron Bioremediation by Utilizing Biochar-Bacterial Composites

Mayank Bahuguna[1], Geeta Bhandari[1], Nupur Joshi[1], Prashant Singh[2], Sanjay Gupta*[1], Saurabh Gangola[3], Shshank Chaube*[4]

[1]School of Biosciences, Swami Rama Himalayan University, Swami Rama Nagar, Dehradun, Uttarakhand, 248016
[2] Department of Chemistry, D. A. V (PG) College, Dehradun, Uttarakhand, India
[3] Department of Microbiology, Graphic Era Deemed to be University, Dehradun, 248002, India
[4] Symbiosis Institute of Technology, Hyderabad Campus, Symbiosis International (Deemed University), Pune, India

***Corresponding authors:** **Shshank Chaube** (shshank.chaube@sithyd.siu.edu.in) and **Sanjay Gupta** (sanjaygupta@srhu.edu.in)

Abstract:

Background- Iron (Fe) contamination in groundwater is a gradual yet significant concern driven by industrial, urban, and agricultural activities, resulting in undesirable organoleptic effects in drinking water. Surface immobilization of bacterial strains onto biochar offers a promising strategy for enhancing adsorption-based remediation.

Purpose- This study investigates the adsorption behaviour of Fe(II) ions using a bacterial-biochar immobilized adsorbent derived from rice husk and *Bacillus subtilis*, isolated from iron-rich soil samples near handpumps located in Haridwar, Uttarakhand, India. The goal was to evaluate the impact on the adsorption capacity for Fe (II) through various sorption and kinetic models, along with material modified properties.

Methods- Rice husk biochar was immobilized with *Bacillus subtilis* and characterized using SEM, BET surface area analysis, and FTIR spectroscopy. Batch adsorption experiments were conducted across Fe(II) concentrations of 10–40 mg/L. Three Sorption kinetics were modeled for fitting the data and similarly three Isotherm behaviors were assessed, supported by regression analyses.

Results- The bacterial-biochar immobilized adsorbent achieved 79.3% Fe(II) removal, outperforming pristine biochar. BET surface areas of 67.76 and 91.84 m^2/g correlated with enhanced adsorption. The FTIR revealed functional groups (alkene: C-H stretching, alcohol: O-H bending, conjugated alkenes: C=C stretching) and metal carbonate structures, provided an insight of active bio sorption sites. A decline in adsorption at higher concentrations, indicated optimal performance at 10–15 mg/L concentration of Fe (II) ions. Kinetic (pseudo-first-order and Weber–Morris intraparticle diffusion) and isotherm (Freundlich and Redlich–Peterson) models validated the presence of heterogeneous adsorption sites.

Conclusions- Surface immobilization of *Bacillus subtilis* onto rice husk biochar significantly enhances Fe(II) adsorption. These findings highlight the potential of bacterial-biochar immobilized adsorbent as a basis for valorization of the green biotechnology usage in groundwater remediation applications.

Keywords: Surface immobilization, Rice Husk, Biochar-Bacterial consortium, Adsorption, Fe (II) ions

1- Introduction

Iron is a prevalent metal in the Earth's crust, primarily existing in two oxidation states: Fe(III) and Fe(II) [1]. While iron is an essential micronutrient necessary for various biological processes, its excess concentration in drinking water can lead to significant health and aesthetic issues. Elevated levels of iron can cause degradation of plumbing fixtures and contribute to organoleptic problems, such as undesirable tastes and staining, ultimately impacting the quality of potable water. The World Health Organization (WHO) recommends a maximum concentration of 0.3 parts per million (ppm) for iron in drinking water, while the Bureau of Indian Standards stipulates a limit of less than 1 ppm (IS 10500 – June 2015 amendments) [2]. The prolonged exposure to elevated Fe concentrations shows major toxicity on human health, including chronic and neurological degradation, hemochromatosis, liver and lung damage, bone fragility, tooth discoloration, skin allergies, and most commonly diarrhoea [3,4]. Unlike the effects of iron accumulation, effective strategies for its removal from aqueous solutions require thorough investigation. Adsorption using natural biosorbents is a physico-chemical treatment that gained traction due to its cost-effectiveness and eco-friendly nature [5]. Recent literature has also illustrated the efficacy of economically derived materials from the agricultural sector in addressing heavy metal contamination in drinking and groundwater [6]. Adsorption stands out among various treatment methods as it avoids the introduction of undesirable by-products into the water, a significant advantage over alternative techniques for iron removal [7]. The efficiency of the adsorption process is influenced by the chemical surface properties of the adsorbents, which play a crucial role in the interaction between metal ions and sorbents [8]. Key factors driving the adsorption of iron include contact time, particle size, and the surface properties of the adsorbent, as well as the kinetics and isotherm models governing the process. The composition of agro-residues rich in lignin and cellulose affects the surface properties and porosity of activated biochar, enabling effective entrapment of metal ions [9]. Particularly, rice-husk biochar based remediation can remove dissolved iron from groundwater through a combination of physicochemical sorption and mineralization processes [10]. Surface oxygenated functional groups (carboxyl, phenolic, hydroxyl) and negatively charged/polar sites binds Fe(II) and Fe(III) by electrostatic attraction, inner-sphere complexation and ligand exchange, further lowering aqueous concentrations [11]. The biochar pore network concentrates solutes and provides abundant nucleation surfaces where hydrolysis and oxidation of iron generate iron oxyhydroxides and other poorly soluble phases that precipitates followed by entrapping within the pores and on the external surfaces [12].

Recent advancements have highlighted the importance of surface modification of different biochar to enhance its efficiency in removing various contaminants, including heavy metals [13]. There is a growing focus on adopting greener approaches in the quest for effective heavy metal removal. Biological methods, particularly bacterial-mediated modifications, are emerging as a promising avenue but still confront challenges related to their efficiency and functionality in large-scale applications [14]. The surface characteristics and functional groups of biochar modulate bacterial interactions via two pathways: a direct effect on cell attachment and activity, and an indirect effect in which high electrical conductivity promotes electron transfer from intracellular oxidation to extracellular reduction during surface immobilization [15,16]. Interestingly, certain bacterial strains in natural environments exhibit remarkable capabilities for the transformation, precipitation, and bioreduction of heavy metals, showcasing their potential as bioremediation agents. At the molecular scale, electron shuttling within the biochar–bacteria composite transfers electrons

from microbial metabolism to acceptors such as Fe(III) oxides, accelerating their reduction and supporting biochar-mediated biomineralization of iron in groundwater [17,18]. The Fe(II) molecules remains soluble unless sequestered by complexation with organic ligands or extracellular polymeric substances (EPS) produced by microbes [19].

This work investigates the performance of biologically modified biochar in removing Fe(II) ions from synthetic groundwater. By mimicking the natural environmental conditions in a controlled laboratory setting, interactions of the bacterial immobilized biochar suitable for groundwater withdrawal systems will provide a sustainable solution for iron contamination and align with global efforts to ensure safe drinking water. Thus, integrating biochar and bacteria within a matrix enables heavy-metal remediation in water systems through complementary mechanisms, including adsorption to biochar surfaces, complexation with functional groups, microbial redox transformation, and biofilm-mediated immobilization along with biomineralization. The concept is already under study in agricultural farm setups, but lacks knowledge in water interactive system, to showcase the bacterial capability for utilizing the heavy metals entrapped on the surface of biochar [20].

Bacterial–biochar composite is a multifunctional assembly in which biochar surface chemistry, attached cells, extracellular polymeric substances (EPS), and any precipitated biominerals together determine heavy-metal fate. EPS and soluble organic compounds can supply abundant binding sites and promote rapid, reversible sorption [21]. In case of specialized microbes, like iron-oxidising (FeOB) and iron-reducing (FeRB) groups of bacteria, $Fe(OH)_3$ gets accumulated in the biofilms at anaerobic interfaces. Abundant surface amino, carbonyl, carboxyl, and hydroxyl functional groups can enhance heavy-metal adsorption onto cell surfaces or within cells in conjunction with a biosorbent [22]. Primarily, the microbiological activity causes oxidation and precipitation of Fe^{2+} on the outer membrane-bound cytochromes under a set of optimal pH and redox potential (Eh), releasing electrons utilized through the Electron Transport chain [23]. Certain examples include *Leptothrix ochracea* and *Gallionella ferruginea* immobilized on sand/ granular activated carbon filter, entrapping Fe oxides on the filter medium [24]. Another mechanism playing a major role in iron uptake involves siderophore production by the neutrophilic biofilm forming bacterial strains, which binds and transports the Fe molecules, enhancing the sequestration ability [25]. Majorly *Bacillus subtilis* exhibits both biofilm formation and specialized siderophore production, displaying traits that contribute to active Fe acquisition from the growth medium and support its normal growth [26].

Immobilizing Bacillus on the rice-husk biochar converts a passive sorbent into an active bioremediation composite [27]. Particularly, the bacillus biofilms establish dense EPS matrix on biochar surfaces that concentrate iron by complexation with EPS functional groups [28]. It further provides microsites of distinct pH and redox potential promoting localized transformation; and enzymatic catalysis or indirect facilitation of redox reactions [29]. It also mediate Fe(III) reduction or stimulate abiotic oxidation by altering local oxygen flux and catalyzing surface redox reactions [30]. Additionally, Biochar itself can facilitate extracellular electron transfer between microbial cells and iron phases, accelerating Fe(II)/Fe(III) interconversion and favoring formation of more stable solid phases on the composite surface [31]. Several recent studies have demonstrated that bacterial immobilization on biochar enhances adsorption, not only occurring through increased surface heterogeneity and biofilm formation but also via active metabolic processes helps in altering contaminant speciation and promote bioprecipitation [22,32,33]. The immobilization by viable vs.

heat-killed bacterial cells is also a topic of research, where the immobilized viable neutrophilic bacterial cells could outperform immobilized non-viable cells for in-situ iron reduction in groundwater treatment systems by altering the local geochemistry [34]. As the water matrices having immobilized living cells maintain active electron transport, metabolic flexibility, and surface chemistry that promote sustained Fe(III) redox transformation, biofilm formation, and self-repair under fluctuating redox and nutrient conditions along with forming stable mineral phases [35]. The localized microenvironments further enhances Fe(III) solubility; immobilization on polymeric beads/matrices, or biochar further enhances the action by stabilizing biomass against hydraulic shear and washout while preserving cell viability and contact with mineral surfaces [36]. Thus, they produce longer-term immobilization, so observed performance in mixed composites often reflects an overlap of immediate EPS-dominated biosorption and later biogenic mineralization [37]. Future studies can thus target for heat-sterilized or chemically inactivated composites, which are prepared identically to the live material [38]. Further areas of research include EPS removal or enzymatic degradation treatments to assess the EPS fraction; time-resolved comparisons of abiotic and biotic reactors to separate rapid sorption from slower biologically mediated changes are some of the possible avenues to explore and deepen the understanding of the exact mechanism [19]. Finally finding a complementary solid-phase analyses by using (SEM-EDS, XRD, FTIR, and sequential extraction) can be utilized to identify biomineral signatures and distinguish sorbed versus precipitated metals [39].

In contrast, non-viable cells or killed biomass rely solely on passive mechanisms such as surface-mediated abiotic electron transfer, reductive dissolution via adsorbed reductants, and reactive functional groups that can catalyse initial iron dissolution [40]. Thus, in the presence of heterogeneous viable immobilized cells a long-term robustness is predicted by competing electron acceptors, fluctuating pH, and oligotrophy, sustaining iron reduction over weeks to months [41]. Whereas, non-viable bacteria are more sensitive to bio-fouling, organic-poor conditions, and loss of reactive surface sites. Operationally, viable immobilized systems require attention to nutrient supply, potential biomass overgrowth, and re-inoculation if repeated sorption-desorption is carried out in a bioremediation system for yielding higher cumulative Fe(II) adsorption and better adaptation to field variability [38]. On the contrary, non-viable systems offer stability and lower biosafety concerns but typically deliver shorter-lived, lower-magnitude iron removal [42]. These constrains can be overcome by exploring a possible avenue of compatible regeneration protocols, including mild chemical buffers, staged reactor designs that separate abiotic regeneration from biological immobilization improvement, and controlled reimmobilization workflows across at least three to five adsorption–desorption cycles to quantify both sorption resilience and microbial functional recovery [13]. For instance, Tao et al. (2018) reported *Bacillus subtilis* immobilized on cotton-stalk biochar contributed to enhanced Cd and Pb immobilization through metabolic transformation and EPS production, whereas heat-killed cells lacked these effects [43]. A recent review by Zhang et al. (2023) further emphasized that viable bacterial biofilms on biochar surfaces facilitate redox transformations, complexation, and microenvironmental shifts that cannot be replicated by non-viable biomass [44].

Furthermore, *Bacillus subtilis* has not been widely studied for the kinetics and isotherm models for Fe adsorption capacity, both in live and dead biomass [45]. On the molecular level, *B.subtilis* confers the biosynthesis ability for bacillibactin via non-ribosomal peptide synthetases (NRPS) which involves the

assembly of 2,3-dihydroxybenzoic acid (DHBA), threonine, and glycine into a cyclic trimeric structure and the enzymes such as DhbA-DhbF catalyzing the formation of bacillibactin [46]. However, the exact mechanism in the case of iron bioremediation by Bacillus strain is underexplored. Though the operational risks for such interventions include: remobilization of iron under shifting pH or reducing conditions, oxidative by-products in the presence of strong oxidants, and hydraulic impairment from precipitate accumulation [22]. These drawbacks can be managed by monitoring Fe speciation, pH, oxidation -reduction potential (ORP), dissolved oxygen-carbon ratio (DOC) and head loss through applying periodic regeneration or backwashing steps [47]. While few studies quote the use of the *Bacillus subtilis* with biochar for studying the effect for heavy metal sorption in the rice plant rhizosphere but still lacks with the specific mechanism in the adsorption process [48]. Furthermore, the adsorption efficiency for other heavy metals, such as Cd(II), Cu(II), Ni(II), Cr(IV), and Pb(II), has been studied using *Bacillus cereus*, and *Bacillus subtilis* with various agricultural residues as immobilizing surfaces, such as rice straw and corn stalk, particularly in the rhizospheric environment [49,50]. The present synthetic groundwater study therefore aims to demonstrates a combined sorption–biotransformation approach analyzed using sorption isotherm and kinetic modelling that maximizes iron retention while aiming for future scope of identifying key process controls required for scale-up and real-world application.

2- Material and Methods

2.1 Collection of Water samples: 23 hand pumps water sampling from 2 districts in Uttarakhand, India was included (i) Haridwar and (ii) Tehri Garhwal District in the study (Table 1). Water samples from the designated sites were collected after pumping for 5 minutes and analyzed using MD 100 Tintometer (Make: Lovibond) for on-site detection of iron concentration and further confirmed using ICP-OES (Agilent Technologies Model no: 5110) as per the standard procedures laid down by the BIS for drinking water. Further the stratified soil samples were collected for isolating the microbial community with a depth of 10cm from the surface near the hand pump spout. The iron concentration ranges detected from field survey were utilized in the further experiments in the Batch system.

Table 1 Iron Concentration in collected Water sample

Sample No.	Site	Tehsil	Coordinates		Iron Conc. (mg/L)	ICP-OES Fe (ppm)
			Lat	Long		
Tehri District						
1	Byasi	Thalisain	30.06°	78.47°	0.83	0.89
2	Singtali	Narendranagar	30.06°	78.45°	0.43	0.42
3	Kaudiyala	Tehri	30.06°	78.50°	0.20	0.17
Haridwar District						
4	Jagjeetpur	Haridwar	30.04°	78.21°	0.35	0.35
5	Missarpur 1	Bahadrabad	29.89°	78.13°	1.53	1.58

6	Jiya Pota	Bahadrabad	29.87°	78.12°	0.38	0.42
7	Nurpur Panjanheri	Bahadrabad	29.88°	78.13°	0.62	0.65
8	Katarpur	Bahadrabad	29.86°	78.12°	0.27	0.27
9	Sarai Jwalapur	Bahadrabad	29.90°	78.09°	1.34	1.35
10	Dandi Chauraha (Bhagtanpur, Abidpur)	Bahadrabad	29.87°	78.07°	0.68	0.70
11	Shubhash Garh	Laksar	29.83°	78.03°	1.90	1.95
12	Aithal	Laksar	29.81°	78.03°	0.03	0.03
13	Baseri	Laksar	29.76°	78.03°	0.42	0.45
14	Akbarpur	Laksar	29.76°	78.06°	0.79	0.80
15	Sultanpur	Laksar	29.75°	78.09°	0.24	0.25
16	Prahladpur	Khanpur	29.68°	77.98°	0.73	0.75
17	Shahpur	Khanpur	29.64°	78.00°	0.07	0.09
18	Khanpur border	Khanpur	29.63°	77.98°	1.76	1.75
19	Laksar Tehsil	Laksar	29.73°	78.01°	0.66	0.65
20	Kaliyar Sharif (Rahmatpur)	South Haridwar	29.90°	77.94°	2.70	2.70
21	Piran Kaliyar	South Haridwar	29.92°	77.93°	0.76	0.78
22	Ghoda Chowk	Bahadrabad	29.92°	78.04°	0.11	0.11
23	Haridwar Highway	Bahadrabad	29.91°	78.08°	0.34	0.35
23	**Total Number of Samples**					

185

186 2.2 Bacterial strains isolation and enrichment: The soil samples were dissolved in a volume of 100ml
187 distilled water, with a weighing ratio of 50 grams. The dissolved soil samples of 1 ml volume were
188 inoculated inside a modified 9K-Spizizen minimal salts – Luria Broth medium [51] prepared into two
189 different components for a total volume of 200 ml (Table 2).

190 **Table 2** Media Components for preparation of 9K - Spizizen minimal salts Medium for bacterial growth.

Media Component A (950 ml), pH=7.0, Autoclaved	Quantity (grams)	**Media Component B (50 ml) Filter sterilized**	Quantity (grams)
Ammonium sulfate; $(NH_4)_2SO_4$	2.0	Ferrous Sulfate Heptahydrate; $FeSO_4 \cdot 7H_2O$	0.139
Potassium Dihydrogen Phosphate,	6.0		

KH_2PO_4	
Dipotassium Phosphate; K_2HPO_4	14.0
Magnesium Sulfate Heptahydrate; $MgSO_4.7H_2O$	0.5
Tri-Sodium Citrate Dihydrate; $Na_3C_6H_5O_7.2H_2O$	1.9
Glucose	5.0
Peptone Powder	10.0
Yeast Extract Powder	5.0
pH	7.5

The broth medium was incubated for 7 days in a shaking incubator (REMI CIS-24 Plus) at 37 °C, 120 rpm. After the completion of the incubation period, the dark brown broth was further enriched on the 9K - Spizizen minimal salts agar medium (1.5% Agar) at pH = 7.5. The loopful culture was streaked and incubated for 48 hours, at a temperature of 37 °C, until yellowish appearance colonies were observed (Fig. 1). After 3 days of incubation, the colonies were sub cultured for obtaining pure cultures.

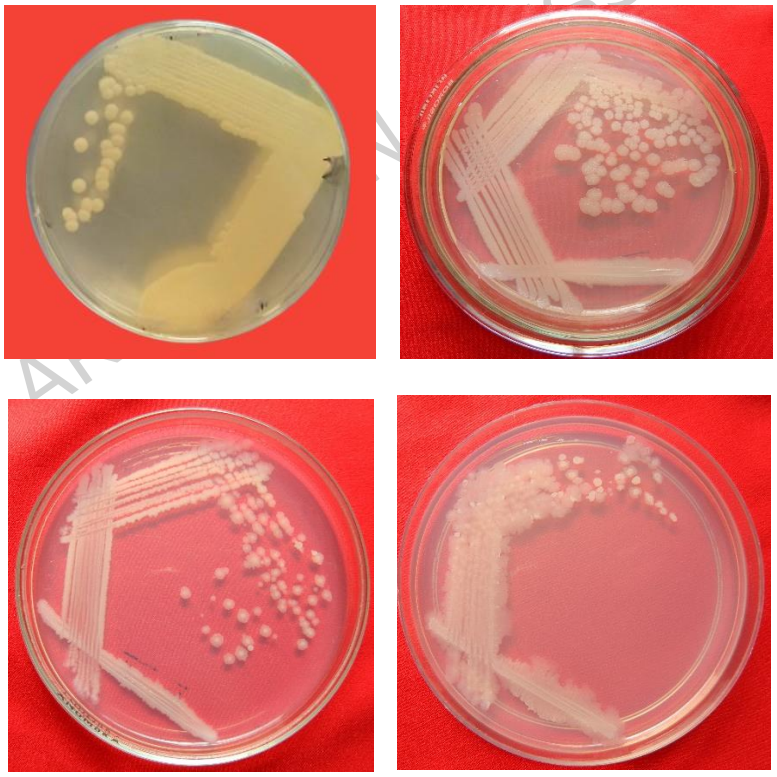

Fig. 1. Pure culture streaked on 9K - Spizizen minimal salts-LB agar medium, (i) IOB-1; (ii) IOB-2; (iii) IOB-3; (iv) IOB-4.

2.3 Morphological Analysis and Identification: The morphological characteristics of the colonies were observed under the microscope at 40X and 100X magnification after gram staining (Fig. 2), and the results were recorded based on the factors of overall shape, size, and arrangement margin of the colonies (Table 3).

Table 3: Morphological characterization of potential iron-reducing bacteria.

Bacterial ID	Morphology	Cell Diameter (μm)
IOB-1	Helical Bacilli	0.26
IOB-2	Curved and helical Bacilli	0.38
IOB-3	Curved and Elliptical Bacilli	0.35
IOB-4	Elliptical and helical Bacilli	0.42

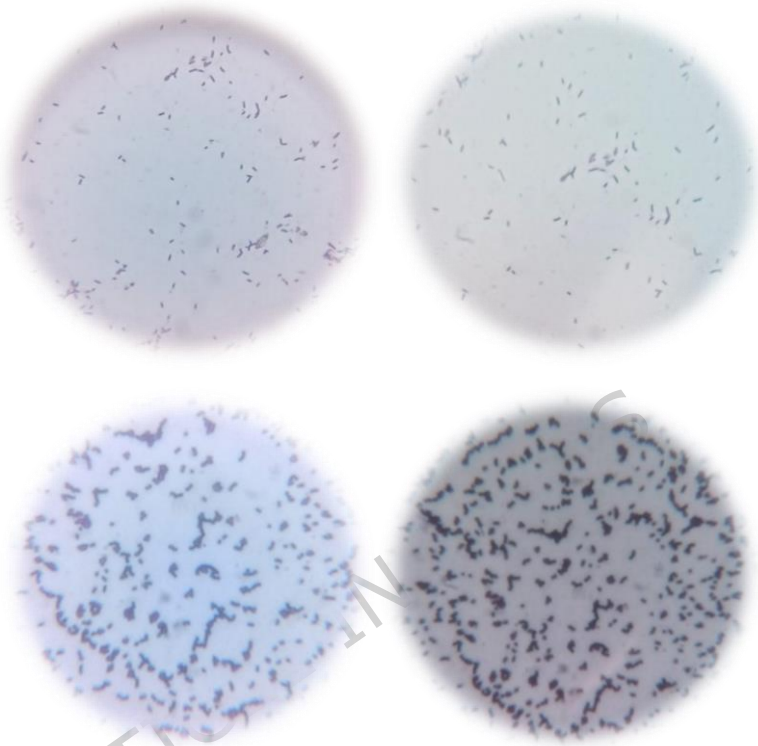

Fig. 2. Gram Staining of isolated bacterial strains, (i) IOB-1; (ii) IOB-2; (iii) IOB-3; (iv) IOB-4.

The agar plates were outsourced for Microbial Identification. Initially, the genomic DNA extraction was done using Chloroform: Isoamyl alcohol-based isolation method from the isolated bacterial cultures and sent to the sequencing facility. DNA quality and concentration in the buffer solution were confirmed from the QC report. A ~1.5 kb 16S rDNA fragment was amplified using a high-fidelity PCR polymerase with the forward primer 5′-CCTACGGGNGGCWGCAG-3′. PCR products were sequenced uni-directionally, and the resulting sequences were aligned and analyzed using PhyloT to identify the bacterial isolate and its closest phylogenetic neighbours (Table 4; Fig. 3). The data was submitted to NCBI SRA portal with Accession Number (PRJNA1338561).

Table 4 Microbial Identification Information

Bacterial Id	Phylogeny	Closest Neighbour
IOB-1	Proteobacteria	*Bacillus subtilis*
IOB-2	Proteobacteria	*Bacillus subtilis*
IOB-3	Proteobacteria	*Bacillus velezensis*

IOB-4	Proteobacteria	*Bacillus cereus*

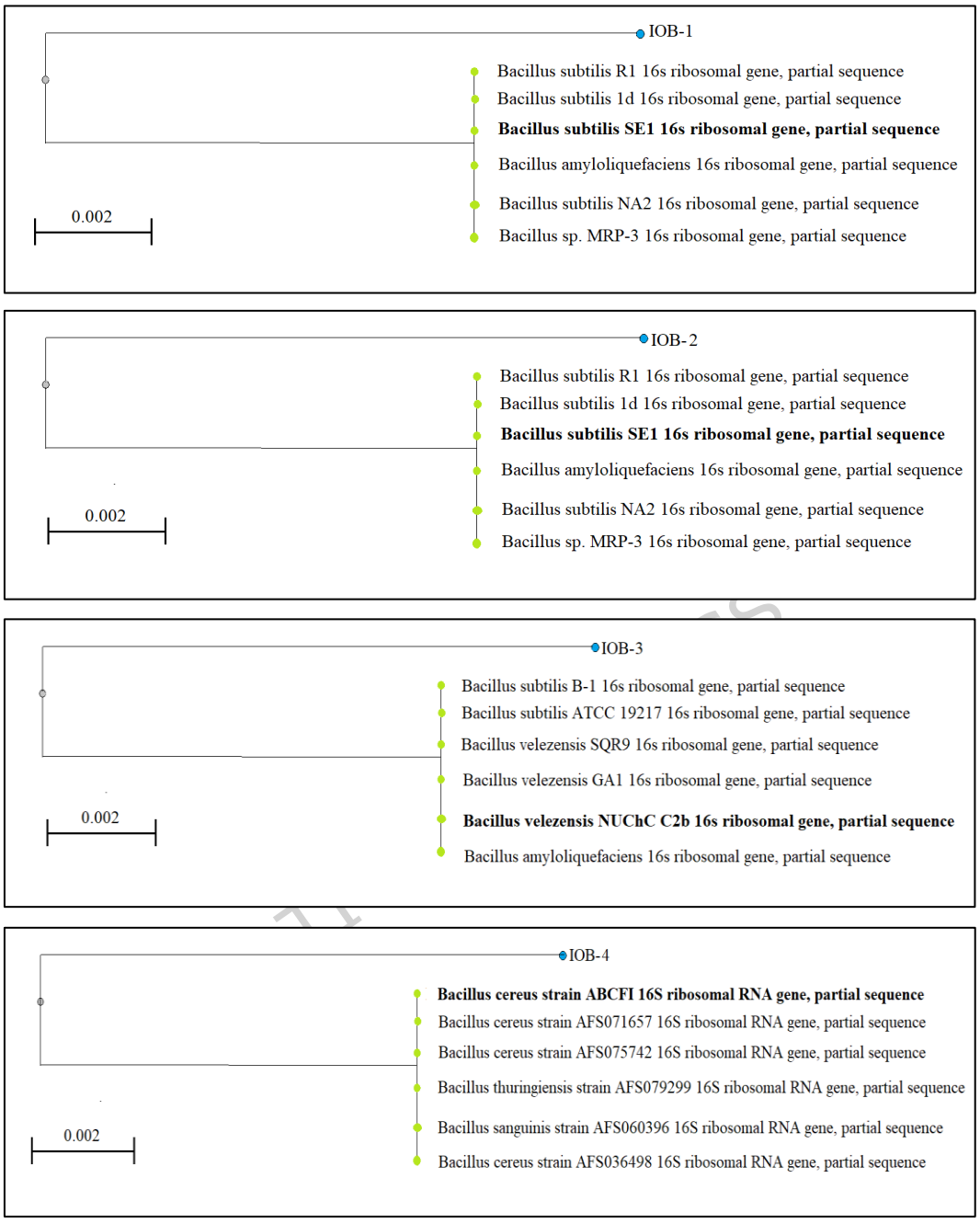

Fig. 3. Phylogenetic tree for closest neighbour, (i) IOB-1; (ii) IOB-2; (iii) IOB-3; (iv) IOB-4.

2.4 Biochar production: The agro-economical waste biomass were selected for biochar production to use as a matrix for bacterial immobilization experiment. The biomass was collected from Dehradun city, Uttarakhand, India. A total of 4 different biomass (rice husk, pineapple peel, sugarcane residue, and spent coffee grinds) material were collected and washed to remove excess dust followed by oven drying to get rid of moisture content at 105 °C inside a hot air oven (REMI RDHO 80). The feedstocks were pyrolyzed under multiple temperature–residence time conditions inside a muffle furnace and compared using proximate

indicators with yield (Table 5). Selection criteria were predefined as: low ash content, adequate yield, development of porous structure (inferred from yield trends and handling integrity), and mechanical stability for downstream immobilization at shorter residence time. Rice husk met these criteria adequately, based on the screening results; where the rice husk biochar used in experiments was produced at 450 °C with a 1-hour residence time.

Table 5 Yield percentage and optimization of pyrolysis conditions.

S.No.	Biomass	Characteristics		
		Pyrolysis Temperature	Residence Time	Yield %
1.	Rice Husk	300°C	3 Hours	35.4%
		350°C	3 Hours	23.5%
		400°C	2 Hours	30.2%
		450°C	1 Hour	37.6%
		500°C	1 Hour	25%
		550°C	0.5 Hour	30.4%
2.	Pineapple Peel	250°C	2 Hours	47.5%
		350°C	1 Hour	37.2%
3.	Sugarcane Residue	300°C	4 Hours	41.6%
		400°C	2 Hours	37.9%
4.	Spent Coffee Grinds	270°C	2 Hours	32.3%
		370°C	0.5 Hour	26.5%

** All reported yields are mean values from triplicate pyrolysis unless otherwise stated*

2.5 Bacterial Loading on Biochar samples: The rice husk biochar sample produced was washed thoroughly to remove the ash residual content, and autoclaved at 121 °C and 15 psi for 20 minutes. One gram of autoclaved biochar was then transferred into a conical flask containing 100 mL of bacterial suspension and incubated for 24 hours at 120 rpm and 30 °C in a shaking incubator (REMI CIS-24 Plus). After incubation, the biochar–bacterial residue was separated by centrifugation at 5,000 rpm for 5 minutes (REMI CPR-24 Plus). The residue was washed with ultrapure water for 3-4 cycles, each with a volume of 50ml (18.2 MΩ - ELGA Ultrapure water system, UK). The washed residue was further oven dried at 40 °C to remove the moisture of the composite (REMI RDHO 80) and stored in an air tight packaging inside refrigerated conditions of 4 °C for further experiments.

The sample with bacterial isolate, IOB-1 nearest neighbour (*Bacillus subtilis*), identified in Table 4, was selected for immobilization based on preliminary qualitative screening for robust compatibility with the biochar matrix. The quantitative enumeration was performed by using 0.03 g bacterial-biochar suspended in 70 mL of sterile saline solution (0.85%) and incubated for 24 hours. The mix was shaken at 150 rpm and checked for cell density at an absorbance of 600 nm read using a (Shimadzu UV-1800 spectrophotometer) [52].

2.6 Characterization of Biochar-Bacterial Composites: The surface and pore characteristics of the biochar composite were analyzed using a BET surface area analyzer (Autosorb iQ-x, S/N: 14713060401, Station 1, version 5.2) to determine the specific surface area and classify pore types. Surface morphology was examined using a scanning electron microscope (SEM; Tescan MIRA 3 LMH), and functional group heterogeneity was assessed by Fourier transform infrared spectroscopy (FTIR; PerkinElmer IV) [43].

2.7 Batch Adsorption Experiment: Ferrous sulfate heptahydrate solutions with concentrations ranging from 10 mg/L to 40 mg/L were prepared in 70 mL volumes of synthetic groundwater for each concentration level [53,54]. The composition of the groundwater was setup for the experiment, based on the study conducted to analyse water quality parameters of Uttarakhand (Table 6).

Table 6 Water Quality Parameters for Uttarakhand [54].

Physicochemical Parameter	Mean Value	BIS Desirable Limit	Metal Salt	Concentration (g/L)
Ca^{2+} (mgL^{-1})	74.05	75	$CaCl_2 \cdot 2H_2O$	0.203
Mg^{2+} (mgL^{-1})	26.06	30	$MgSO4 \cdot 7H_2O$	0.260
Na^{+} (mgL^{-1})	3.03	_	NaCl	0.008
K^{+} (mgL^{-1})	1.26	200	KCl	0.032
Cl^{-} (mgL^{-1})	16.48	250	NaCl	0.028
NO_3^{-} (mgL^{-1})	4.10	45	$NaNO_3$	0.0069
SO_4^{2-} (mgL^{-1})	55.06	200	Na_2SO_4	0.044
pH	7.62	6.5–8.5	NaOH/ HCl	7.5

The experiment consisted of reaction mixture made up in a volume of 70ml with 0.03 gram of biochar-bacterial composite, and incubated 120 rpm at 30°C for 24 hours (REMI CIS-24 Plus Shaking Incubator). The solution was filtered through a Millipore filtration assembly (0.22 µm) and analyzed by ICP-OES (Agilent Technologies, Model 5110) at a wavelength of 238.2 nm.

The factors of effect of pH, temperature and biochar dosage were conducted for the following ranges of initial culture medium pH (pH 5.0–8.0), incubation temperature (25, 30, 35 °C), and Biochar dosage (10-40mg) which were tested for their effect on Fe(II) removal. The experiments were conducted in triplicate. The tests were performed in 70 mL synthetic wastewater supplemented with 14.72 mg/L {~15 mg/L) of Fe(II). Furthermore, the resulting data from iron concentration variation was fitted to kinetic and isotherm models using initial iron concentrations of 10, 15, 20, 25, 30, 35, and 40 mg/L, with contact times of 30 minutes, 1–5 hours, and equilibrium measurements up to 24 hours. Each adsorption experiment was conducted in triplicate to minimize experimental error, and a blank sample of synthetic groundwater without adsorbent served as the control. The reported residual Fe concentrations and removal percentages are mean values from triplicate experiments.

The amount of Fe(II) ions adsorbed per gram of biochar and the percentage removal were calculated using the following equations (1) and (2):

$$q_e = \frac{(C_0 - C_e) \times V}{m}$$

$$\% \text{ Removal} = \left(\frac{C_o - C_e}{C_o}\right) \times 100 \quad (2)$$

where, C_o and C_e are the initial and equilibrium Fe(II) concentrations (mg L^{-1}) respectively. q_e is the equilibrium adsorption capacity (mg g^{-1}), m is the dry weight of the biochar samples (g), and V is the volume of total reaction mixture (L) [55–57].

The sorption isotherm was studied for the period of 24 hours using 4 different models, (1) Langmuir: explaining monolayer sorption equilibrium of Fe (II) on the biochar's homogenous surface [58]; (2) Freundlich: displaying a heterogeneous sorption equilibrium of Fe (II) on the biochar surface [59]; and (3) Temkin: representing heterogeneous distribution of binding energies based on the heat of adsorption occurring with Fe (II) ions due to their interaction with various functional groups on the biochar [60]. (4) Redlich Peterson: explains adsorption sites having varying affinities for the Fe (II) ions [61].

Langmuir isotherm model linear and non-linear representation are written as equations (3) and (4):

$$\frac{C_e}{q_e} = \frac{C_e}{q_m} + \frac{1}{K_L q_m} [Linear\ Langmuir] \quad (3)$$

$$q_e = \frac{q_m K_L C_e}{1 + K_L C_e} \ [Non - Linear\ Langmuir] \quad (4)$$

where, q_m is the monolayer biosorption capacity of Fe (II) ions on biochar surface (mg g^{-1}) and K_L is the Langmuir constant (L mg^{-1}) which are determined from the linear plot of C_e/q_e Vs C_e. The Langmuir isotherm parameters also consider a dimensionless factor of separation factor 'R_L' which is used to predict the affinity of surface modified biochar for Fe (II) ions; expressed in the equation (5).

$$R_L = \frac{1}{1 + K_L C_o} \quad (5)$$

A separation factor (R_L) value between 0 and 1 indicates favourable adsorption of Fe(II) ions, R_L >1 denotes unfavourable adsorption, R_L = 1 corresponds to linear adsorption, and R_L = 0 represents an irreversible adsorption process.

Freundlich isotherm model linear and non-linear form is expressed as equations (6) and (7):

$$\ln q_e = \ln K_F + \frac{1}{n} \ln C_e \ [Linear\ Freundlich] \quad (6)$$

$$q_e = K_F C_e^{\ 1/n} \ \ [Non - Linear\ Freundlich] \quad (7)$$

where, K_F is the Freundlich constant determined from the intercept of the linear plot of ln q_e Vs ln C_e, while the slope of the plot corresponds to (1/n) ratio representing the sorption intensity of the biochar respectively.

Temkin isotherm model linear equation (8) is represented as:

(8)

$$q_e = B \ln A_T + B \ln C_e \; [Linear\ Temkin]$$

where, A_T is the Temkin isotherm equilibrium binding constant (L g^{-1}) and B is defined as constant related to heat of sorption (J mol^{-1}). These parameters are obtained from the intercept and slope, respectively, of the linear plot of ln q_e Vs C_e.

Further for the non-linear isotherm form, Redlich-Peterson model was utilized as equation (9):

$$q_e = \frac{K_R C_e}{1 + a_R C_e{}^{n}} \quad [Non - Linear\ Redlich\ Peterson] \tag{9}$$

where, K_R explains the Redlich-Peterson isotherm rate constant, and n stands for the dimensionless exponent factor, along with (a_R) which is regarded as Redlich-Peterson coefficient. These values are determined by the intercept and slope in q_e Vs. C_e plot.

The sorption kinetics was studied based on two models of Fe (II) ions, (1) Pseudo-first-order: representing *physisorption* of Fe (II) complexes into the pores of biochar and (2) Pseudo-second-order: representing *chemisorption* of Fe (II) ions with the functional groups on biochar surface. Additionally, Webber Morris intraparticle diffusion was studied representing boundary layer contribution in the diffusion model. The data comparison of the experimental and predicted values will display the best of model and its relevance.

Pseudo-first-order (PFO) kinetics model linearized and non-linearized equations (10, 11) are expressed as [62]:

$$\ln(q_e - q_t) = \ln(q_e) - k_1 \cdot t \quad [Linear\ PFO] \tag{10}$$

$$q_t = q_e(1 - e^{-k_1 t}) \quad [Non - linear\ PFO] \tag{11}$$

where, q_t is the amount of Fe(II) adsorbed per unit mass of biochar at time t (mg g^{-1}) and k_1 is the pseudo first order rate constant (min^{-1}), calculated from the slope of the linear plot of log (q_e - q_t) Vs time.

Pseudo-second order (PSO) kinetics model linearized and non-linearized equations (12, 13) are expressed as [63]:

$$\frac{t}{q_t} = \frac{1}{k_2 {q_e}^2} + \frac{t}{q_e} \quad [Linear\ PSO] \tag{12}$$

$$q_t = \frac{{q_e}^2 k_2 t}{1 + q_e k_2 t} \quad [Non - Linear\ PSO] \tag{13}$$

where, $h = k_2 q_e{}^2$ is the initial sorption rate of Fe (II) ions and k_2 is the pseudo second order rate constant. Both of these values are determined by plotting t/qt Vs time.

Furthermore, Webber Morris intraparticle diffusion model in linearized equation (14) is expressed as:

$$q_t = k_{id} \cdot t^{0.5} + C \quad [Linear\ Webber - Morris] \tag{14}$$

where, q_t is the adsorption capacity of Fe(II) ions on biochar at time t (mg g^{-1}) and k_{id} is the intraparticle diffusion rate constant; and [C] represents the boundary layer effect. The parameters were obtained from the slope k_{id} and intercept C value on the plot of $t^{0.5}$ Vs q_t.

3- Results & Discussion-

3.1 Biochar Characteristics: The biochar samples were characterized using BET, SEM-EDX, and FTIR analysis. BET analysis indicated that the biochar samples followed a Type IV isotherm model. A rapid increase in adsorption within the P/P_0 range of 0–0.1 suggested that micropores played a dominant role in this initial phase. In the P/P_0 range of 0.1–1.0, adsorption increased progressively with relative pressure, reflecting the contribution of mesoporous surfaces. The nearly parallel adsorption-desorption branches over a wide relative pressure range resembled an H4 hysteresis loop, confirming the coexistence of micropores and mesopores in the biochar material. Such Type IV behaviour and H4 hysteresis commonly indicate a hierarchical micropore–mesopore network in biomass-derived carbons, which typically enhances adsorption of aqueous metal ions by combining high specific area with possible transport pathways [64].

For pristine rice husk biochar, the BET surface area was 67.76 $m^2 g^{-1}$, with a micropore surface area of 38.73 $m^2 g^{-1}$, accounting for 57 % of the total surface area. In contrast, the bacterial-biochar composite exhibited a 35 % increase in BET surface area to 91.84 $m^2 g^{-1}$, with a micropore surface area of 45.61 $m^2 g^{-1}$, representing 49 % of the total surface area (Table 7).

Table 7 Physical properties of biochar.

Specific Surface Properties	Pristine Rice Husk Biochar	Biochar-Bacterial Composite
BET surface area (m^2/g)	67.76	91.84
Micropore area (m^2/g)	38.73	45.61
Total pore volume (cm^3/g)	0.05	0.068
Micropore volume (cm^3/g)	0.018	0.021
Average pore diameter (nm)	2.36	2.21

The observed 35% increase in BET surface area, together with the smaller relative contribution of micropore area (from 57% to 49%), indicates that bacterial immobilization generated additional mesoporous features while partially altering the micropore network. Mechanistically, the microbial colonization could have lead to possible EPS deposition and mild biomass-derived surface restructuring widening the pore diameter through micro-to-mesopore transitions, producing the observed decrease in average pore diameter and increase in total pore volume [65]. Both micropores and mesopores therefore serve as principal adsorption sites in the biochar, and the combined increase in surface area and pore volume plausibly provides a greater number of adsorption sites while improving mass-transfer access within the biochar matrix. BET and BJH are bulk textural metrics; complementary pore imaging (e.g., high-resolution TEM) or NLDFT/N2-adsorption advanced analysis would better resolve micro/mesopore connectivity and is recommended for follow-up studies.

SEM analysis revealed abundant grooves and pores that facilitated microbial colonization, with numerous dispersed and aggregated bacterial cells observed within the porous network (Fig. 4). These surface features are known to enhance mass transfer and provide loci for sorption and possible micro-precipitation in biochar–microbe composites [66]. Furthermore, the increased presence of small precipitates on the biochar surface in the post-modification stage corresponded to a higher adsorption efficiency for the target contaminant. The EDX data along with SEM images provided the elemental variation of Carbon, Oxygen, Nitrate and Sulfur components in different samples (Table 8).

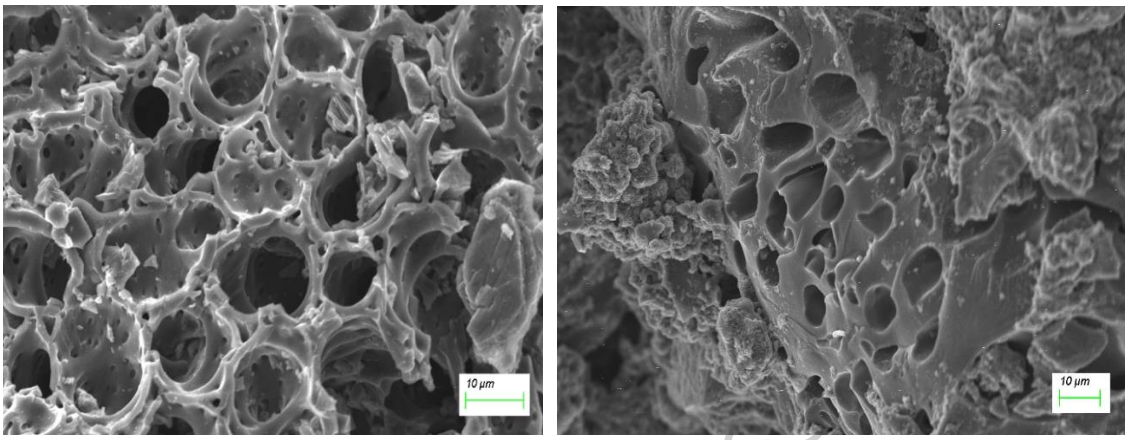

Fig. 4. SEM images of Rice Husk Biochar (1) Pristine Biochar; (2) Bacterial-Biochar Composite

Table 8 Elemental composition analysis for biochar samples.

	Pristine Biochar		**Bacterial-Biochar Composite**	
Elemental Composition	Weight %	Atomic %	Weight %	Atomic %
Carbon	34.5	43.6	33.6	45.5
Oxygen	51.9	49.1	39.7	40.3
Aluminum	11.1	6.2	2.5	1.5
Sulphur	1.5	0.7	21.7	11
Potassium	0.7	0.3	0.6	0.11
Calcium	0.4	0.1	1.9	0.9

FTIR analysis revealed that both pristine and modified biochar exhibited the same characteristic peaks with corresponding vibrational modes. A broad peak at 3422 cm^{-1} was assigned to hydroxyl (–OH) and alcohol functional groups bound via hydrogen bonding. Hydroxyl and surface-bound water bands often increase in intensity following biofilm formation or organic loading, reflecting the possible EPS and cellular contributions to surface chemistry [66].

In the bacterial–biochar composite, a distinct peak at 3094 cm^{-1} corresponded to C–H stretching in alkene groups, indicating the presence of organic functional groups potentially involved in biosorption or microbial attachment at the biochar surface following immobilization [43,67]. The new or increased bands at ~3094 cm^{-1}, ~1640 cm^{-1} and ~1409 cm^{-1} are consistent with organic coatings or EPS released during

bacterial growth and have been associated with enhanced metal binding through carboxylate and proteinaceous ligands [68]. The 1640 cm^{-1} band may reflect conjugated C=C stretches and/or proteinaceous (amide-I like) contributions [43], while the 1409 cm^{-1} band was assigned to O–H bending indicating the carbonate-type vibrations or with carboxylate functional groups that can arise from organic coatings or EPS in the bacterial–biochar composite, which may lead to tentative formation of carbonate mineral phases after treatment [15,48,69]. Further the peak of 1037 cm^{-1} corresponded to S=O stretching in sulfoxides, suggesting the presence of sulfur-reduction groups, potentially linked to methionine sulfoxide reductases that play a critical role in oxidative stress responses in *Bacillus sp.* [70]. This band requires targeted biochemical assays and are therefore speculative in this study. Finally, the peak at 801 cm^{-1} was assigned to Si–O–Si stretching, reflecting the silica content of rice husk biochar, which may contribute to enhanced adsorption efficiency (Fig. 5). Overall, FTIR changes are consistent with increased organic coatings and surface functionalisation after bacterial immobilization, which plausibly increase the density of carboxylate, hydroxyl and sulfur-containing binding sites relevant for Fe(II) removal.

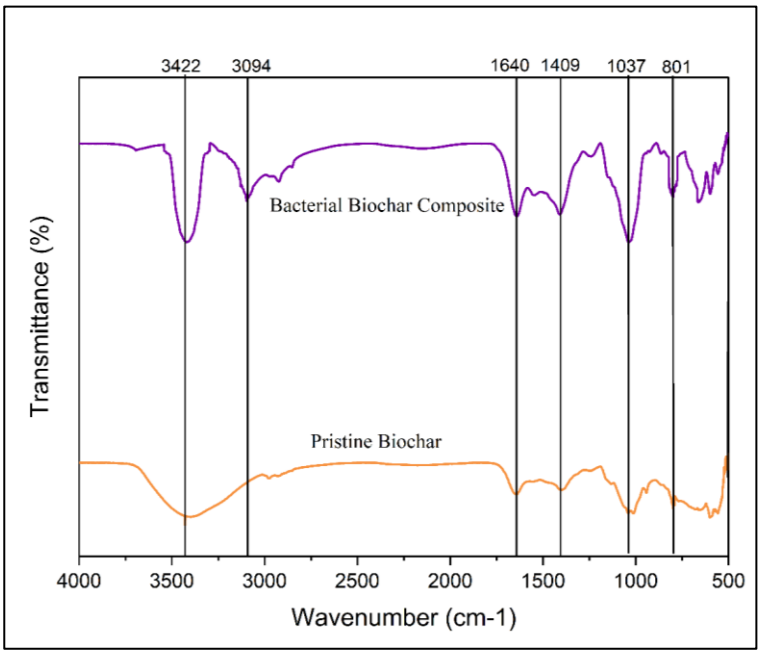

Fig. 5. FTIR Plot of Bacterial immobilized biochar and Pristine Rice husk Biochar.

3.2 Adsorption Experiments:

3.2.1 Effect of different factors on Iron adsorption- The influence of initial pH, biochar dosage and incubation temperature on Fe(II) removal was evaluated for both pristine biochar (PB) and the bacterial–biochar composite (BBC). Across the tested pH range, both biochar samples showed low removal under acidic conditions (pH 5.0), with BBC removing 7.7% and PB 12.7%. Removal increased toward near-neutral pH and reached a maximum for BBC at pH 7.5 (75.1% versus 63.5% for PB). Both adsorbents produced an alkalinizing effect on the solution during contact, with BBC consistently yielding slightly higher final pH values. For instance, at initial pH 6.0 the final pH for BBC was recorded as 6.21 vs PB 5.70; and at initial pH 7.5 the final pH of BBC (7.65) vs PB (7.49) displayed a little variation tending towards the stability. The factor of Relative standard deviations (RSD) across the triplicates were modest (BBC ≈2.6–4.1%; PB ≈0.35–

418 4.6%), supporting reproducibility of the observed pH trend. These results indicate a favourable operating
419 window around pH 6.0–7.5 with empirical peak at pH 7.5, where reduced proton competition and possible
420 surface oxidation/precipitation pathways enhanced the Fe(II) uptake, especially for the BBC [71] [Suppl.
421 Figure 1 (A)]. Furthermore, dose-response experiments showed that increasing biochar mass reduced the
422 residual Fe concentration and increased removal for both materials, with an optimal dosage near 0.03 g under
423 the present conditions. At 0.01 g residual Fe concentrations were 9.05 $mg \cdot L^{-1}$ (PB) and 6.92 $mg \cdot L^{-1}$ (BBC)
424 (38.5% and 53.0% removal, respectively). The best performance was observed for 0.03 g of biochar where the
425 Fe residual of 5.19 mg·L−1 in PB, for average Fe calculated concentration calculated with efficiency of 64.8%
426 removal. Further BBC residual 3.66 $mg \cdot L^{-1}$; 75.1% removal displayed a better reduction. Above 0.03 g both
427 biochar samples showed a small decline in percent removal (BBC 71.3% at 0.035 g and 67.5% at 0.04 g),
428 consistent with diminishing returns and particle-packing or aggregation effects that can reduce accessible
429 surface area at higher loadings [65] [Suppl. Figure 1 (B)].

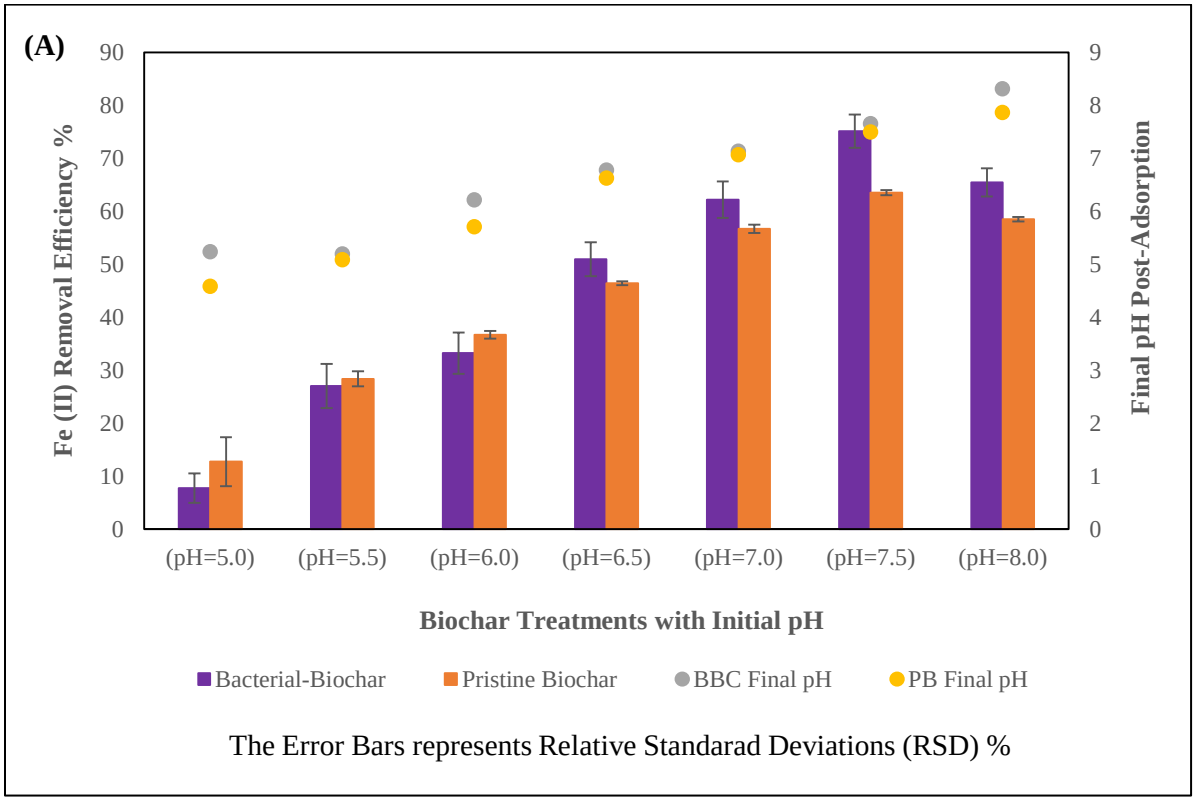

430

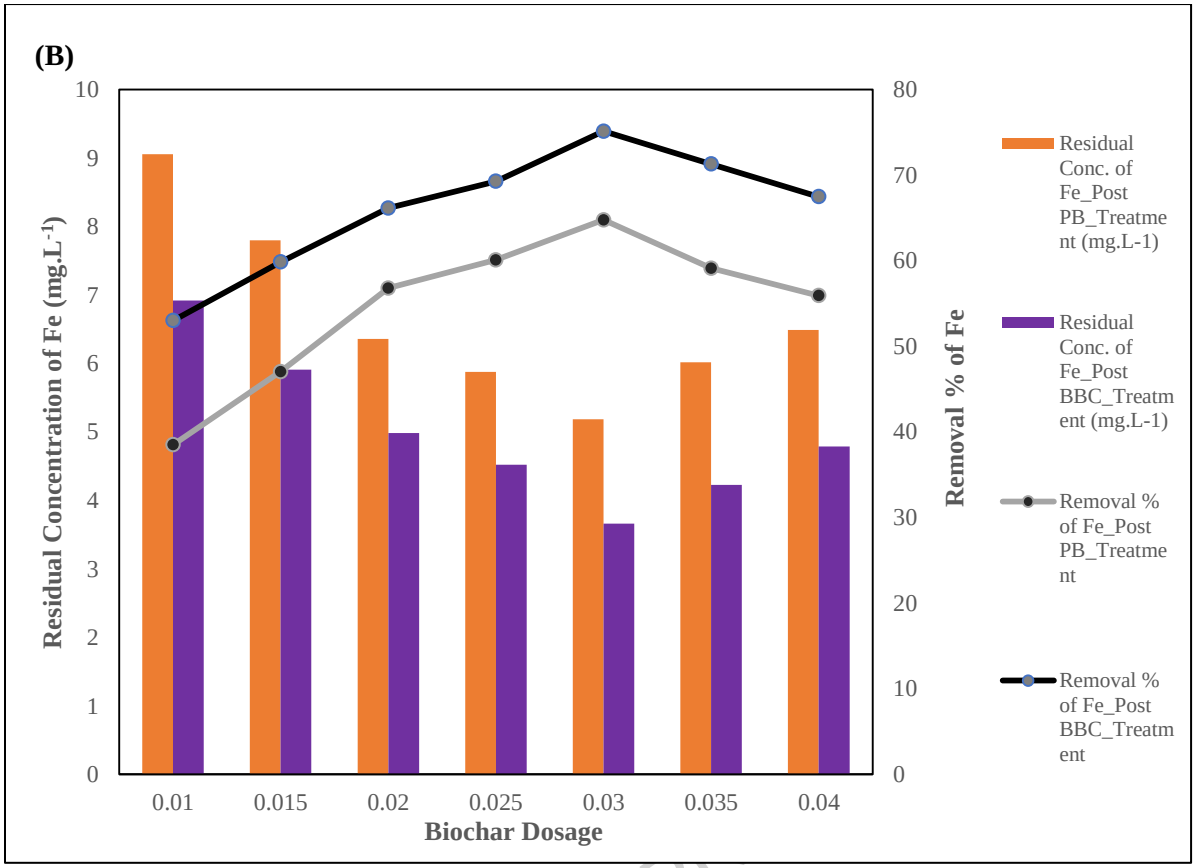
(B)
Residual Concentration of Fe (mg.L-1)
Removal % of Fe
Biochar Dosage
0.01
0.015
0.02
0.025
0.03
0.035
0.04
Residual Conc. of Fe_Post PB_Treatment (mg.L-1)
Residual Conc. of Fe_Post BBC_Treatment (mg.L-1)
Removal % of Fe_Post PB_Treatment
Removal % of Fe_Post BBC_Treatment

431

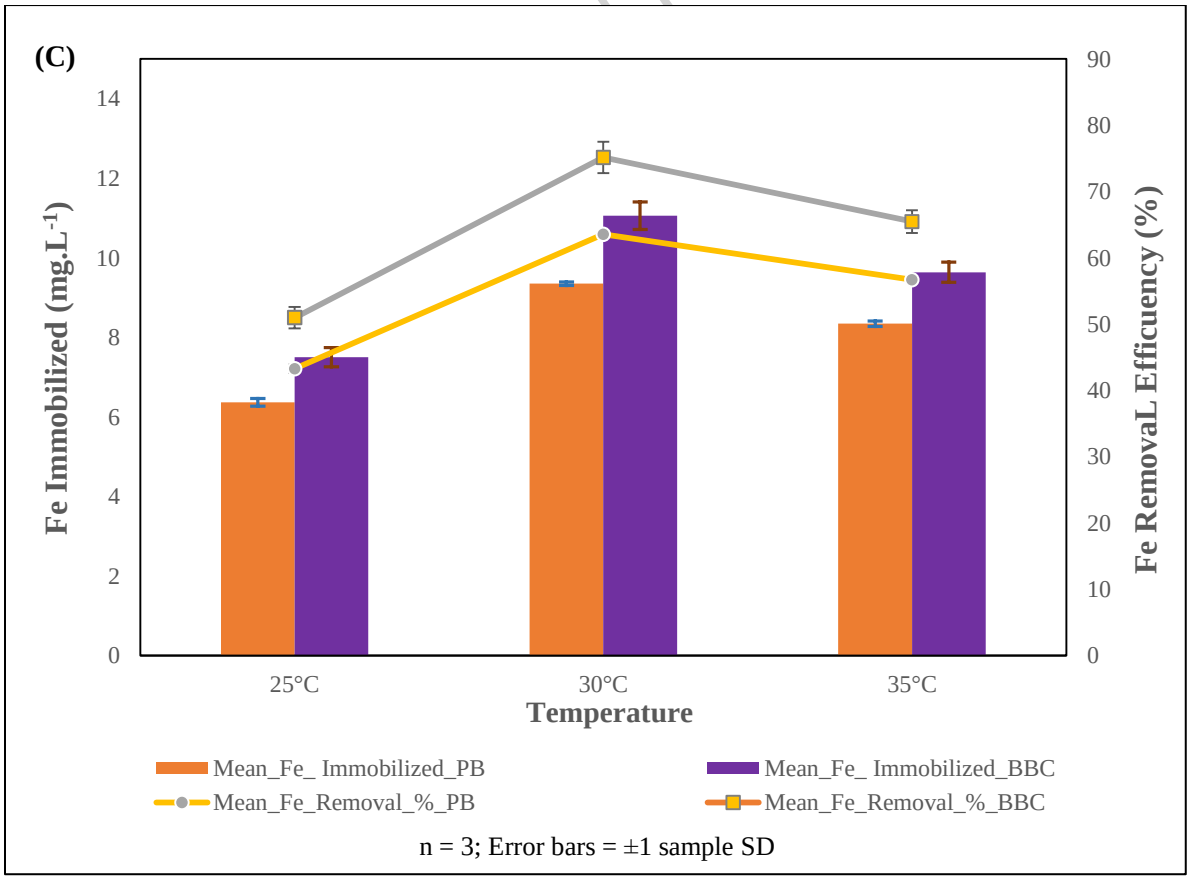
(C)
Fe Immobilized (mg.L-1)
Fe RemovaL Efficuency (%)
25°C
30°C
35°C
Temperature
Mean_Fe_ Immobilized_PB
Mean_Fe_ Immobilized_BBC
Mean_Fe_Removal_%_PB
Mean_Fe_Removal_%_BBC
n = 3; Error bars = ±1 sample SD

432

Supplementary Fig. 1 Effect of different (A) initial and final pH; (B) Biochar Dosage; (C) temperature on Fe (II) immobilization in synthetic groundwater medium.

The experiment for operating temperature optimization at 25, 30 and 35 °C displayed the optimized parameter at 30 °C where both the treatments showed their best performance. BBC immobilized 11.06 $mg \cdot L^{-1}$ Fe with 75.12% removal (SD 2.37%), and PB immobilized 9.35 $mg \cdot L^{-1}$ with 63.52% removal (SD 0.30%). Lower immobilization at 25 °C and 35 °C (BBC: 7.50 $mg \cdot L^{-1}$; 50.96% at 25 °C and 9.63 $mg \cdot L^{-1}$; 65.45% at 35 °C) suggests an interplay of temperature effects on reaction kinetics, microbial activity (for BBC) and sorption equilibria that favours mild warming without thermal deactivation [22]. The three temperatures were chosen to bracket typical laboratory and mild environmental conditions (ambient to slightly elevated) and clearly identify a practical optimum at 30 °C without claiming broader thermal behavior [Suppl. Figure 1 (C)]. The improved performance of BBC across pH, dose and temperature series likely reflects combined effects of (i) increased accessible surface area and mesoporosity after immobilization, (ii) additional functional groups and EPS that provide carboxylate/hydroxyl/sulfur binding sites, and (iii) micro-scale processes including surface oxidation and localized precipitation that remove Fe(II) from solution. The consistent alkalinizing shift and better performance of BBC near neutral pH are compatible with proton consumption at surface sites and formation of surface-bound iron oxyhydroxides or carbonates; however, definitive assignment of precipitated iron phases requires complementary speciation (XRD/XPS) and mapping analyses [72].

3.2.2 Linear Adsorption Isotherm Model- The experimental equilibrium data were fitted into 3 linearized isotherm models for understanding the adsorption mechanisms. All three linearized models delivered high correlation coefficients for the tested concentration range, indicating that aspects of monolayer adsorption, heterogeneous surface binding and adsorbent–adsorbate interactions contribute to Fe(II) uptake (Table 9; Fig. 6) [73].

Table 9 Langmuir, Freundlich and Temkin adsorption isotherm parameters for Fe (II) adsorption by Pristine and Bacterial-Biochar composite sample.

Adsorbent	Linear Isotherm model and parameters						
	Langmuir		Freundlich		Temkin		
	qmax (mg/g)	R^2	1/n	R^2	B_T (J mol^{-1})	K_T (L mg^{-1})	R^2
Pristine Biochar	57.80	0.98	0.61	0.97	18.6	1.01	0.99
Bacterial-Biochar	59.52	0.98	0.35	0.99	8.08	0.86	0.97

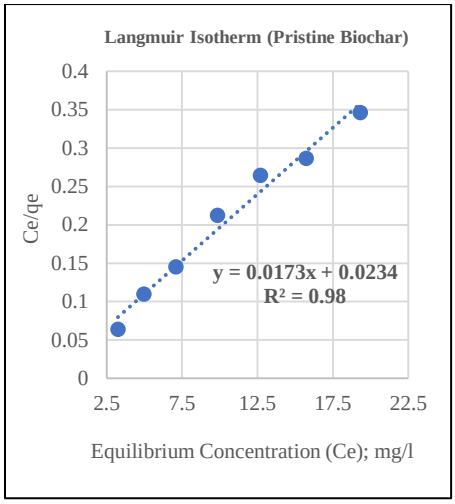

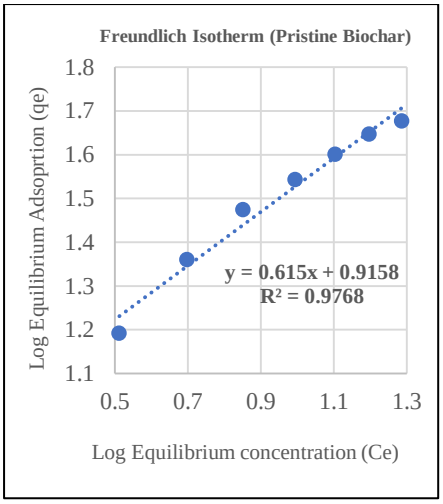

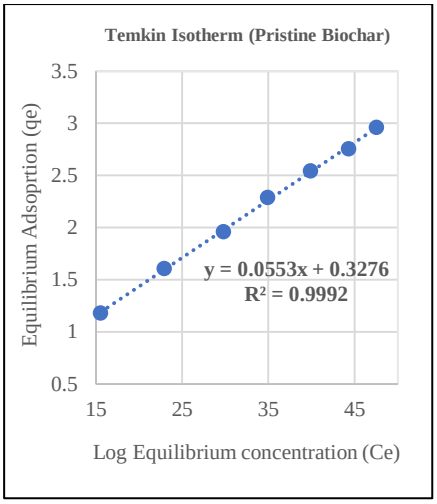

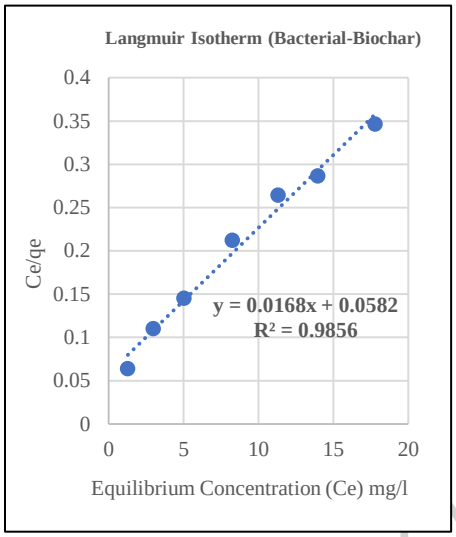

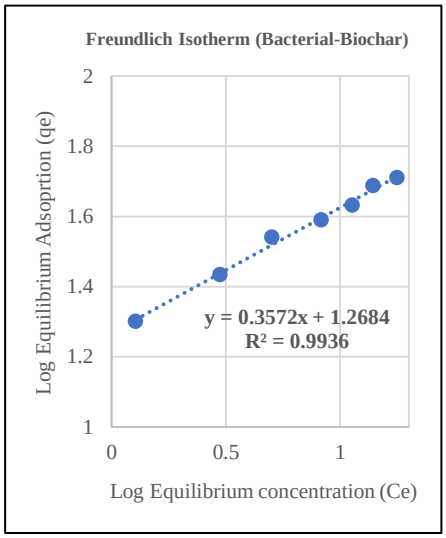

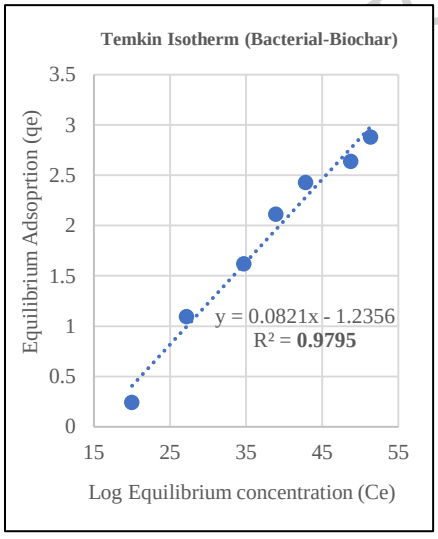

Fig. 6. Linear adsorption isotherm of Fe (II) molecule with different concentrations of Fe_2SO_4 in Pristine and Bacterial-Biochar composite modification. The data points correspond to the experimental measurements, while the dotted lines represent the fitted curves based on the Langmuir, Freundlich, and Temkin isotherm models.

Langmuir parameters suggest substantial maximum sorption capacities (qmax ~ 57.8–59.5 $mg \cdot g^{-1}$ in the linear fit), while Freundlich 1/n values indicate surface heterogeneity and favourable adsorption (Table 9). The Temkin parameters (B_T, K_T) further implied that adsorbent–adsorbate interactions are energetically non-uniform, consistent with a mixed mechanism combining specific binding sites and multilayer/heterogeneous uptake [74]. Taken together, the linear fits indicate that the system cannot be described solely by an ideal monolayer on a homogeneous surface and that heterogeneity introduced by the bacterial immobilization alters adsorption energetics. The isotherm fitting used mean equilibrium concentrations from triplicate experiments

3.2.3 Non-Linear Adsorption Isotherm Model-

The non-linear isotherm model for Fe (II) adsorption displayed mixed-mechanism, heterogeneous adsorption for both materials with superior description by Redlich–Peterson and Freundlich models (R^2 = 0.99; χ^2_reduced PB = 0.014, BBC = 0.037). Pristine biochar exhibits a higher Langmuir q_m (77.49 $mg \cdot g^{-1}$) whereas bacterial biochar shows higher apparent affinity (K_L = 0.316; K_F = 18.735) and markedly greater heterogeneity (Freundlich, n = 2.83). The bacterial composite's lower R_L range (0.07–0.24) confirms more favourable uptake at tested initial concentrations. Taken together, these results indicate that bacterial treatment shifted adsorption energetics toward fewer but stronger high-affinity sites and increased surface heterogeneity, favouring multilayer and non-uniform binding at low concentrations rather than a simple increase in classical monolayer site density. This trade-off has practical implications where BBC may perform better at low contaminant concentrations and for short contact times where high-affinity sites and heterogeneous binding dominate, while PB may retain larger theoretical q_{max} under ideal monolayer assumptions (Table 10). The separation factor (R_L) indicated favourable adsorption with bacterial-biochar. Furthermore, it also record a higher 1/n ratio explaining the presence of a more heterogeneous adsorption surface in the freundlich isotherm model, with a ratio of 2:1, in contrast with pristine biochar. The bacterial-biochar parameter of goodness of fit from χ^2 displayed a variation in results where, both the Freundlich and Redlich–Peterson models exhibit excellent fits with low χ^2_red values (0.033 and 0.037) and high R^2 (0.99), indicating strong predictive accuracy and surface heterogeneity. In contrast, the Langmuir model shows a higher χ^2_red (0.262) and lower R^2 (0.92), suggesting it is less suitable for describing the adsorption behavior (Fig. 7).

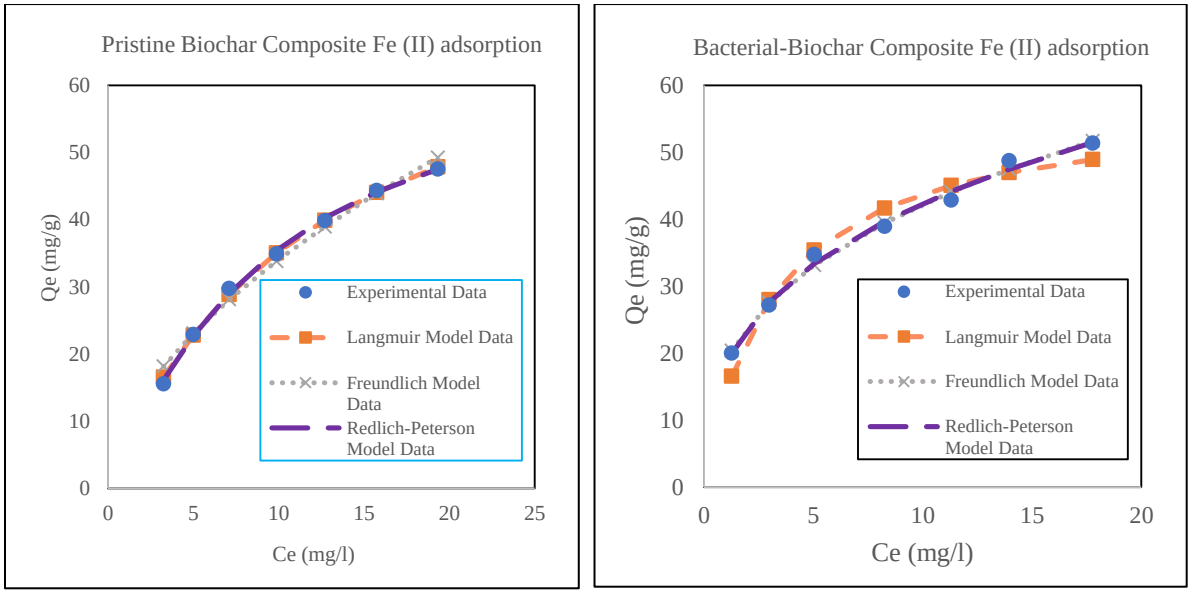

Fig. 7. Non-linear adsorption isotherm of Fe (II) molecule with different concentration of Fe_2SO_4 in Pristine and Bacterial-Biochar composite modification. Data points represent the experimental measurements, while the dotted lines correspond to the non-linearly fitted Langmuir, Freundlich, and Redlich-Peterson isotherm models.

Additionally, the Low Chi Square (χ^2) value indicated excellent fit with overall little deviation across all points. Reduced $\chi^2 < 1$ confirmed minimal unexplained variance and normalizes the deviation by the degrees of freedom. The models were checked with the appropriate fitted parameters and data points in the experiment. These values confirm the statistical robustness of the fitted isotherm and support its mechanistic plausibility.

Table 10 Non-linear adsorption isotherm parameters for Fe (II) adsorption by Pristine and Bacterial-Biochar composite sample.

Samples	**Langmuir**		**Freundlich**		**Redlich-Peterson**	
Pristine	q_m (mg/g)	77.49	n	1.78	n	1.17
Biochar	K_L	0.083	K_f	9.408	K	5.810
	R^2	0.99	R^2	0.98	a	0.04
	R_L	0.17 - 0.46	χ^2	0.6019	R^2	0.99
	χ^2	0.097	χ^2_reduced	0.120	χ^2	0.056
	χ^2_reduced	0.019			χ^2_reduced	0.014
Bacterial	q_m (mg/g)	57.58	n	2.83	n	0.67
Biochar	K_L	0.316	K_f	18.735	K	147.16
	R^2	0.95	R^2	0.99	a	7.10
	R_L	0.07 - 0.24	χ^2	0.165	R^2	0.99

χ^2	1.239	χ^2_reduced	0.033	χ^2	0.151
χ^2_reduced	0.2478			χ^2_reduced	0.037

3.2.4 Linear Adsorption Kinetic Model-

Kinetic experiments were used to probe the rate-controlling steps for Fe(II) uptake by pristine biochar (PB) and bacterial–biochar composite (BBC). Both biochar showed increasing Fe(II) uptake with contact time, up to 300 minutes. BBC exhibited a higher removal efficiency of 56.06% at an Fe(II) concentration of 35 mg L^{-1} in the synthetic groundwater compared to PB. Across the other Fe(II) concentrations series, the bacterial-biochar consistently showed superior removal, with efficiencies of 79.39% (10 mg L^{-1}); 75.87% (15 mg L^{-1}); 66.29% (20 mg L^{-1}); 56.93% (25 mg L^{-1}); 56.17% (30 mg L^{-1}); 52.14% (40 mg L^{-1}), respectively (Fig. 8). Linearized kinetic fits were performed using pseudo-first-order (PFO), pseudo-second-order (PSO) and Weber–Morris intraparticle diffusion models (Table 11) [75]. In the linear fits, the PFO and Weber–Morris intraparticle diffusion model gave high correlation coefficients ($R^2 \approx 0.98–0.99$) for PB, whereas BBC displayed a stronger overall uptake (higher q_e value ~ 104.16) but poorer agreement with the PSO linear fit (reduced R^2 relative to PB, i.e. 0.93) (Fig. 9).

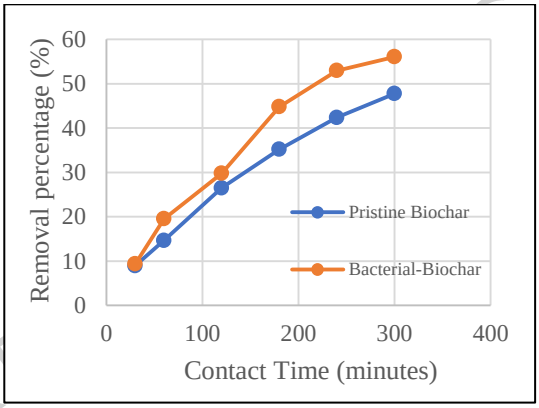

Fig. 8. Influence of contact time on percentage removal of Fe(II) through Pristine and Bacterial-Biochar composite Rice Husk biochar with adsorbent dosages 30 mg; (0.15 mg/ml); Fe (II) concentration 35 mg/L; Temp. 30 °C.

Furthermore, BBC shows higher apparent q_e values across models (linear $q_e \approx 62.7$ mg·g^{-1} for BBC vs ≈ 49.5 mg·g^{-1} for PB in the PFO linear fit, consistent with its larger accessible surface area and added functional groups. The Weber–Morris plots indicate that intraparticle diffusion contributes to Fe (II) uptake, but is not the sole rate-limiting step thus, multi-linearity and non-zero intercepts suggests both boundary-layer and intraparticle contributions playing their role in this case [76]. The faster initial uptake of Fe (II) using BBC implies stronger high-affinity sites or enhanced film-diffusion at early times. Taken together, the linear kinetic analysis supports a multi-step uptake mechanism involving film diffusion, surface sorption and slower intraparticle transport rather than a single simple rate law [77].

Table 11 Linear adsorption Kinetics model data for Fe (II) on Pristine and Bacterial-biochar composite.

Adsorbent	Kinetic model and parameters							
	Pseudo Ist Order			Pseudo IInd Order			Webber Morris	
	q_e	K_1 (min^{-1})	R^2	q_e	K_2 (mg/g.min)	R^2	K_{id} (mg/h.min)	R^2
Pristine Biochar	49.49	0.0069	0.98	80	3.87E-05	0.98	0.3652	0.99
Bacterial-Biochar	62.72	0.0097	0.98	104.16	2.65E-05	0.93	0.2946	0.98

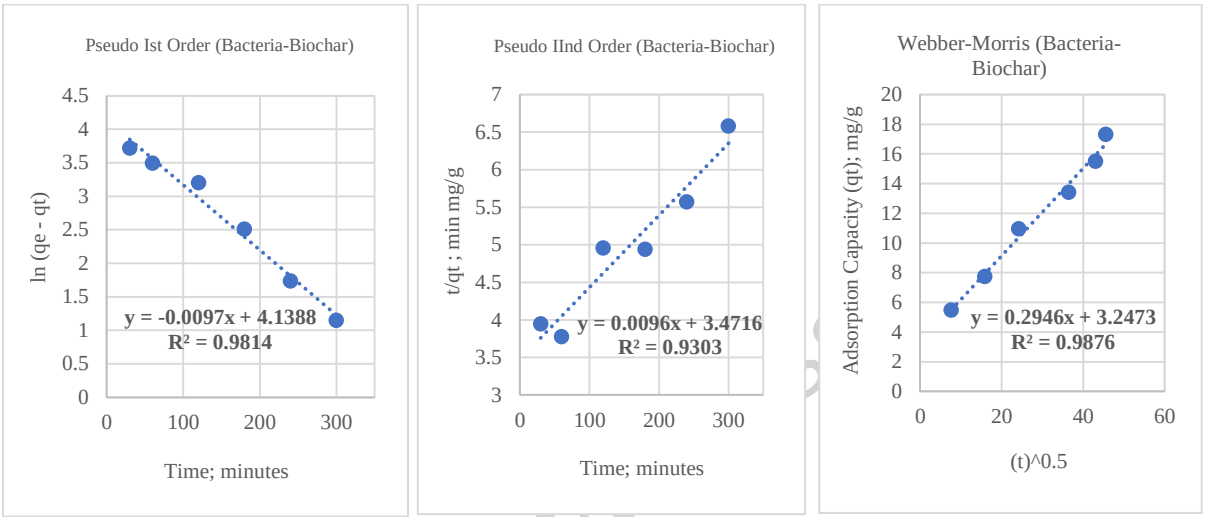

Fig. 9. Linear adsorption kinetics of Fe (II) molecule with different concentration of Fe_2SO_4 in Pristine and Bacterial-Biochar composite modification. The data points represent the experimental values, while the dotted lines correspond to the fitted curves of the pseudo-first-order, pseudo-second-order, and Weber–Morris kinetic models.

3.2.5 Non-linear Adsorption Kinetic Model-

Non-linear kinetic modelling was performed using the non-linear forms of the PFO and PSO equations to preserve the original error structure and derive robust parameter estimates. The PSO model displayed a higher equilibrium adsorption capacity (q_e = 83.85 for PB, 98.75 mg.g^{-1} in BBC), compared to the PFO (q_e = 53.22, 62.67 mg/g) with significant R^2 values for both the models (Table 12). Further analysis of PB kinetics showed slightly lower RMSE (0.315) and χ^2 (5.35*10^{-5}) than the PFO fit, indicating a marginally better description of the full time-series by the PSO model (Fig. 10). On the contrary, the PSO model suggests higher adsorption capacity and PFO model showed comparable or slightly better statistical accuracy for BBC, implying that multiple kinetic regimes may coexist in the composite material.

Table 12 Non-linear adsorption Kinetics model data for Fe (II) on Pristine and Bacterial-biochar composite.

Adsorbent	Kinetic model and parameters

	Pseudo Ist Order					Pseudo IInd Order				
	q_e	K_1 (min^{-1})	R^2	RMSE	Chi-Square	q_e	K_2 (mg/g.min)	R^2	RMSE	Chi-Square
Pristine Biochar	53.22	0.0043	0.99	0.355	0.001	83.85	3.421E-05	0.99	0.315	5.35E-05
Bacterial-Biochar	62.67	0.0045	0.99	1.3388	0.048	98.75	3.068E-05	0.98	1.423	0.069

The higher non-linear q_e values from PSO fitting are consistent with a dominant chemisorption component under some conditions. However, model preference varied between biochar performances and must be interpreted alongside the Weber–Morris intraparticle diffusion results and surface characterization. Thus, the overall kinetic behavior is best described as multi-step explain, a rapid initial uptake controlled by film diffusion and high-affinity surface sites, followed by slower intraparticle diffusion and equilibration that may include surface complexation and local precipitation processes [78].

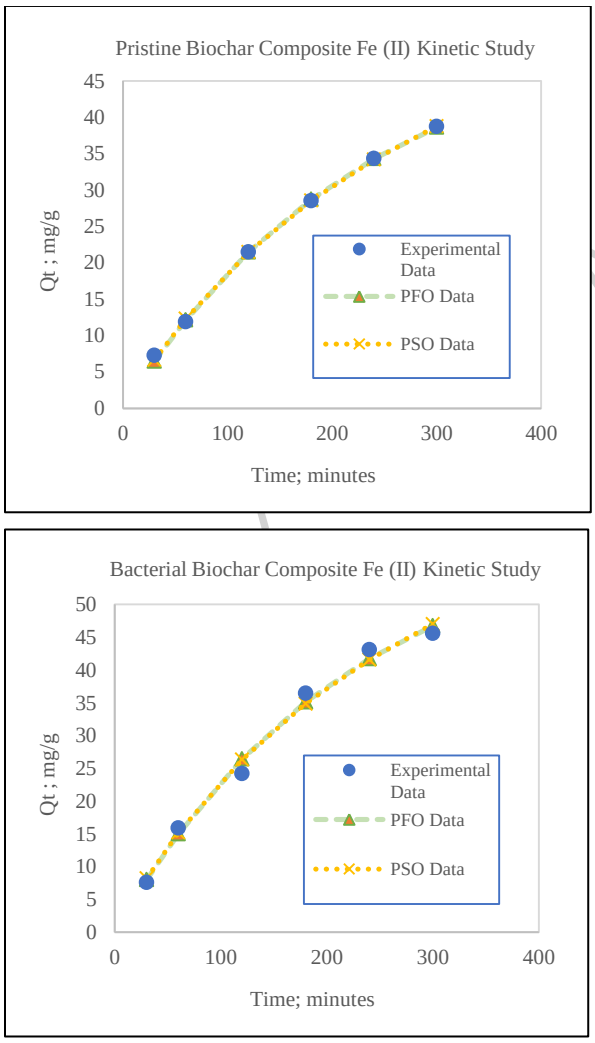

Fig. 10. Non-linear adsorption kinetics of Fe (II) molecule with different concentration of Fe_2SO_4 in Pristine and Bacterial-Biochar composite modification. The data points correspond to the experimental results, while

the dotted lines depict the fitted curves for the non-linear representation of pseudo-first-order and pseudo-second-order kinetic models.

4- Conclusion-

The study characterized rice husk biochar immobilized with bacterial culture to evaluate its efficiency for Fe (II) biosorption compared to pristine biochar from synthetic groundwater across pH, dosage and temperature series, along with isotherm and kinetic modelling for equilibrium and variable contact time. The synthetic groundwater composition was matched with the chemical analyses of field samples collected from the same survey area to reproduce dominant ionic strength, pH and representative dissolved organic carbon, along with previous reported study. The findings of this study support the use of bacterial biosorbents derived from agricultural waste as an effective and cost-efficient strategy for reducing heavy metal pollution in aquatic systems. The bacterial-biochar composite displayed a BET surface area increase by 35 % (91.84 vs 67.76 $m^2 \cdot g^{-1}$) in comparison to pristine biochar sample and developed a more heterogeneous micro/mesoporous network. The changes with faster initial uptake, higher apparent affinity in non-linear isotherm fits, and better removal efficiency near neutral pH (empirical peak at pH 7.5) provided an advantage. The convergent evidence from non-linear isotherm and kinetic modelling together with FTIR drives a clear, three-stage mechanistic picture for Fe(II) removal by the bacterial–biochar composite (BBC). The initial rapid removal of Fe (II) was well supported by Non-Linear Isotherm Data, followed by high-affinity surface binding phase evidenced from reduction of bacterial biochar at 30 minutes and 60 minutes in the contact time experiment and large non-linear PSO q_e of 98.75 $mg \cdot g^{-1}$ for BBC). The second stage was evidenced with secondary heterogeneous/multilayer uptake of Fe (II) ions into accessible mesopores supported by (high Freundlich isotherm rate constant K_F = 18.73; and total pore volume range variance from 0.05 to 0.068 $cm^3 \cdot g^{-1}$ after immobilization). The final slow equilibration stage controlled by Weber–Morris multi-linearity, observed alkalinizing pH shifts of 7.5 to 7.65 and SEM-EDX showing increased surface Sulfur (S) weight % of 1.5 to 21.7. These mechanistic inferences are explicitly supported by data points achieving ~79% removal at the optimized batch dose (0.03 g at C_0 = 10 $mg \cdot L^{-1}$), and showed peak performance near pH 7.5 at 30 °C up to 24 hours at equilibrium with isotherm achieved with 87% removal and residual Fe concentration of 1.273 $mg \cdot L^{-1}$.

Overall, the results highlight the considerable potential of bacterial biochar composite, to serve as a possibly efficient biosorbent for Fe(II) removal from groundwater. The findings contribute substantially to the growing range of bioremediation methods, highlighting the vital role of agro-waste valorization in advancing environmental management practices. This research also defines a concise, actionable roadmap to advance validation and deployment. Targeted post-adsorption characterization on adsorbed Bacterial-biochar composite (XRD for phase identification, XPS for Fe(II)/Fe(III) speciation, and SEM-EDX mapping for spatial co-localization) should be undertaken to quantify the relative contributions of sorption versus surface precipitation. Replicating column tests with unfiltered field groundwaters representing different DOC, hardness and redox regimes are needed to produce breakthrough curves at multiple EBRTs (initially ranging from 5 to 30 minutes), from which minimal effective bed depth, mass-transfer zone length and time-to-breakthrough can be derived. Regeneration and lifecycle protocols should be evaluated over at least five successive cycles of desorption using mild chemical elution, nutrient pulses or low-temperature

desorption; and endpoints including retained removal efficiency, viable cell fraction (plate counts/qPCR or live/dead assay) and finally biochar mass loss per cycle. Concurrently, quantifying the bacterial leaching in column effluents ($CFU \cdot mL^{-1}$ and qPCR); screening effluents and regeneration eluates with standard aquatic ecotoxicity assays to support safe handling or post-treatment requirements. Multi-contaminant testing (Fe with Mn, As, representative cations and NOM) to determine competitive effects and operational selectivity. Finally, integrating empirical results into a techno-economic model and comparative benchmarking (levelized cost per m^3; sensitivity to adsorbent life and regeneration frequency) against aeration-filtration and ion exchange to inform pilot design and deployment choices suitability.

Supplementary Table: Comparison of Cost Implications and Commercialization Feasibility for future studies of Biochar Based sorbents for Water Treatment [79,80].

Method	**Remediation Performance**	**Representative cost metric ($USD \cdot m^{-3}$)**	**Commercialization Feasibility**	**Cost-benefit interpretation**
Aeration-Filtration	Fe removal typically 70–99% depending on feed and filter configuration (oxidation followed by particulate capture)	Low–moderate capital and generally the lowest OPEX among conventional options; typically, 0.20 to 0.80 $USD \cdot m^{-3}$	High feasibility for municipal and community systems; simple operation and low skill needing favor wide adoption. Performance drops with high DOC or complex groundwater matrices, requiring pre/post-treatment.	Strong cost-performance ratio where dissolved Fe is present and water matrix allows rapid abiotic oxidation; low chemical waste and simple operation make benefits high vs cost.
Ion Exchange (Resin)	Very high removal (90–99%) on proper selection for dissolved Fe species under appropriate speciation/competing cation conditions	Higher OPEX due to resin regeneration and brine disposal; typically, 1-3 $USD \cdot m^{-3}$	Commercially mature for industrial/polishing units; and less attractive for decentralized units	High removal reliability but ongoing chemical/regenerant costs and secondary waste streams reduce net benefit
Membrane filtration (NF/RO)	Very high removal (95–99.9%) across species; effective but sensitive to fouling and feed quality	High CAPEX and high OPEX (energy - membrane replacement; typically, 2-6 $USD \cdot m^{-3}$	Feasible for centralized treatment where budgets, energy and pretreatment are available	Excellent performance but high lifecycle costs and fouling/regeneration burdens reduce cost-benefit in many groundwater contexts.
Adsorbent: conventional iron-oxide modified activated carbon	High measured capacities (80–99%) for iron/other metals in lab studies for batch experiments	Cost varies by material in lab and pilot studies show wide ranges; typically, 0.50-5.00 $USD \cdot m^{-3}$	Commercially feasible where adsorbent lifetime and local feedstock cost permit low per-treatment cost	Adsorbents can deliver high removal at small scale; cost-benefit depending on material manufacture cost, regeneration ability and life.

Bacillus–biochar composite (In our study)	87.3% removal from C0 = 10 mg L^{-1} to Ce ≈ 1.273 mg L^{-1} after 24 h (biotic + sorptive hybrid pathway) ➢ Composite dose = 0.01 $kg.m^{-3}$ ➢ Composite lifetime = 50 $m^3.kg^{-1}$ ➢ Implied material cost =28.18 $USF.kg^{-1}$ ➢ Material cost contribution = 0.2818 $USD.m^{-3}$	Per-kg commercial cost requires further modelling. Natural treatment systems along with (constructed-wetland style) central sample averages capital ≈ US$609 per kl/day and O&M ≈ US$800 per kl/day (total ≈ US$1,409 per kl/day) for decentralized nature-based systems	Commercialization feasibility hinges on four factors: (1) Composite lifetime and regeneration; (2) Local agro-waste pyrolysis with low-cost inoculum; (3) Regulatory acceptance for use of live microbes; (4) Governance and business model to capture external benefits	Mechanistically promising at lab scale: hybrid removal can be competitive with aeration-filtration when considering combined sorption + biotic precipitation

Author Contributions

Mayank Bahuguna: Data curation, Formal analysis, Investigation, Methodology, Validation, Visualization, Writing-original draft, Writing-review and editing; **Geeta Bhandari:** Methodology, Data Validation; **Nupur Joshi**: Conceptualization, Data curation, Investigation, Methodology, Review & Editing; **Prashant Singh**: Project Administration, Resource Management and Supervision; **Sanjay Gupta**: Methodology, Investigation, Data Validation, Supervision; **Saurabh Gangola**: Methodology, Data Validation; **Shshank Chaube:** Formal analysis, Validation, Visualization.

Funding: This work was funded by the Uttarakhand Council for Biotechnology, India.

Declarations

The authors have no competing interests to declare that are relevant to the content of this article.

Consent for Publication

Not Applicable

Ethics Approval and Consent to Participate

Not Applicable

Data Availability

The data is available on the NCBI SRA submission portal with accession number PRJNA1338561.

References-

1. Xia X, Teng Y, Zhai Y. Biogeochemistry of Iron Enrichment in Groundwater: An Indicator of Environmental Pollution and Its Management. Sustainability. 2022 Jun 9;14(12):7059. Available from: https://www.mdpi.com/2071-1050/14/12/7059

2. WHO. Guidelines for drinking-water quality, volume 2: Health criteria and other supporting information. Vol. 61, Science of The Total Environment. 1996. p. 274.

3. Heikkinen K, Saari M, Heino J, Ronkanen AK, Kortelainen P, Joensuu S, et al. Iron in boreal river catchments: Biogeochemical, ecological and management implications. Sci Total Environ. 2022 Jan;805:150256. Available from: https://linkinghub.elsevier.com/retrieve/pii/S004896972105333X

4. Briguglio M, Hrelia S, Malaguti M, Lombardi G, Riso P, Porrini M, et al. The Central Role of Iron in Human Nutrition: From Folk to Contemporary Medicine. Nutrients. 2020 Jun 12;12(6):1761. Available from: https://www.mdpi.com/2072-6643/12/6/1761

5. Richards S, Dawson J, Stutter M. The potential use of natural vs commercial biosorbent material to remediate stream waters by removing heavy metal contaminants. J Environ Manage. 2019 Feb;231:275–81. Available from: https://linkinghub.elsevier.com/retrieve/pii/S0301479718311472

6. Divyabharathi R, B. K, J.S. SSR, Chinnasamy S. Recent advances in sustainable agro residue utilisation, barriers and remediation for environmental management: Present insights and future challenges. Ind Crops Prod. 2024 Sep;216:118790. Available from: https://linkinghub.elsevier.com/retrieve/pii/S0926669024007672

7. Younas F, Younas S, Bibi I, Farooqi ZUR, Hameed MA, Mohy-Ud-Din W, et al. A critical review on the separation of heavy metal(loid)s from the contaminated water using various agricultural wastes. Int J Phytoremediation. 2024 Feb 23;26(3):349–68. Available from: https://www.tandfonline.com/doi/full/10.1080/15226514.2023.2242973

8. Singh V, Ahmed G, Vedika S, Kumar P, Chaturvedi SK, Rai SN, et al. Toxic heavy metal ions contamination in water and their sustainable reduction by eco-friendly methods: isotherms, thermodynamics and kinetics study. Sci Rep. 2024 Mar 31;14(1):7595. Available from: https://www.nature.com/articles/s41598-024-58061-3

9. Bhardwaj A, Bansal M, Garima, Wilson K, Gupta S, Dhanawat M. Lignocellulose biosorbents: Unlocking the potential for sustainable environmental cleanup. Int J Biol Macromol. 2025 Mar;294:139497. Available from: https://linkinghub.elsevier.com/retrieve/pii/S0141813025000467

10. Li Z, Zheng Z, Li H, Xu D, Li X, Xiang L, et al. Review on Rice Husk Biochar as an Adsorbent for Soil and Water Remediation. Plants. 2023 Mar 31;12(7):1524. Available from: https://www.mdpi.com/2223-7747/12/7/1524

11. Severo FF, da Silva LS, Moscôso JSC, Sarfaraz Q, Rodrigues Júnior LF, Lopes AF, et al. Chemical and physical characterization of rice husk biochar and ashes and their iron adsorption capacity. SN Appl Sci. 2020 Jul 25;2(7):1286. Available from: https://link.springer.com/10.1007/s42452-020-3088-2

12. Li C, Wang S, Du X, Cheng X, Fu M, Hou N, et al. Immobilization of iron- and manganese-oxidizing bacteria with a biofilm-forming bacterium for the effective removal of iron and manganese from groundwater. Bioresour Technol. 2016 Nov 1 [cited 2023 Jul 28];220:76–84. Available from: https://pubmed.ncbi.nlm.nih.gov/27566515/

13. Feng NJ, Kong LJ, Huang MZ, Diao ZH. Recent Advances Toward Biochar Immobilized Microorganisms for the Remediation of Heavy Metals from Water and Soil: A Review. Water, Air, Soil Pollut. 2025 Mar 24;236(3):178. Available from: https://link.springer.com/10.1007/s11270-025-07821-6

14. Azad D, Pateriya RN, Arya R, Sharma RK. Biological Treatment for Biochar Modification: Opportunities, Limitations, and Advantages. In: Engineered Biochar. Singapore: Springer Nature Singapore; 2022. p. 85–104. Available from: https://link.springer.com/10.1007/978-981-19-2488-0_6

15. Ouyang P, Narayanan M, Shi X, Chen X, Li Z, Luo Y, et al. Integrating biochar and bacteria for sustainable remediation of metal-contaminated soils. Biochar. 2023 Oct 5;5(1):63. Available from: https://link.springer.com/10.1007/s42773-023-00265-3

16. Zhao J, Li F, Cao Y, Zhang X, Chen T, Song H, et al. Microbial extracellular electron transfer and strategies for engineering electroactive microorganisms. Biotechnol Adv. 2021 Dec;53:107682. Available from: https://linkinghub.elsevier.com/retrieve/pii/S0734975020301841

17. Pascual MB, Sánchez-Monedero MÁ, Cayuela ML, Li S, Haderlein SB, Ruser R, et al. Biochar as electron donor for reduction of N2O by Paracoccus denitrificans. FEMS Microbiol Ecol. 2020 Aug 1;96(8). Available from: https://academic.oup.com/femsec/article/doi/10.1093/femsec/fiaa133/5865124

18. Kappler A, Wuestner ML, Ruecker A, Harter J, Halama M, Behrens S. Biochar as an Electron Shuttle between Bacteria and Fe(III) Minerals. Environ Sci Technol Lett. 2014 Aug 12;1(8):339–44. Available from: https://pubs.acs.org/doi/10.1021/ez5002209

19. Sonkar M, Nag K, Mahapatra K, Chandra V, Sankhyan S, Ray S, et al. Recent advances in bacterial extracellular polymeric substances mediated heavy metal removal: an eco-friendly and innovative approach. Bioremediat J. 2024 Dec 19;1–24. Available from: https://www.tandfonline.com/doi/full/10.1080/10889868.2024.2440752

20. Bolan S, Hou D, Wang L, Hale L, Egamberdieva D, Tammeorg P, et al. The potential of biochar as a microbial carrier for agricultural and environmental applications. Sci Total Environ. 2023 Aug;886:163968. Available from: https://linkinghub.elsevier.com/retrieve/pii/S0048969723025895

21. Zeng W, Li F, Wu C, Yu R, Wu X, Shen L, et al. Role of extracellular polymeric substance (EPS) in toxicity response of soil bacteria Bacillus sp. S3 to multiple heavy metals. Bioprocess Biosyst Eng. 2020 Jan 23;43(1):153–67. Available from: http://link.springer.com/10.1007/s00449-019-02213-7

22. Amabilis-sosa LE, Valenzuela EI, Quezada-renteria JA, Pat-espadas AM. Biochar-Assisted Bioengineered Strategies for Metal Removal : Mechanisms , Key Considerations , and Perspectives for the Treatment of Solid and Liquid Matrixes Keywords : Sustainability. 2022;14(17049):1–20. Available from: https://www.mdpi.com/2071-1050/14/24/17049

23. Tothero GK, Hoover RL, Farag IF, Kaplan DI, Weisenhorn P, Emerson D, et al. Leptothrix ochracea genomes reveal potential for mixotrophic growth on Fe(II) and organic carbon. Bose A, editor. Appl Environ Microbiol. 2024 Sep 18;90(9). Available from: https://journals.asm.org/doi/10.1128/aem.00599-24

24. Thinojah T, Ketheesan B. Iron removal from groundwater using granular activated carbon filters by oxidation coupled with the adsorption process. J Water Clim Chang. 2022 May 1;13(5):1985–94. Available from: https://iwaponline.com/jwcc/article/13/5/1985/88548/Iron-removal-from-groundwater-using-granular

25. Kanamarlapudi K, Ramya SL, Sudhamani M. Structural Changes of Bacillus subtilis Biomass on Biosorption of Iron (II) from Aqueous Solutions: Isotherm and Kinetic Studies. Polish J Microbiol. 2019;68(4):549–58. Available from: https://www.sciendo.com/article/10.33073/pjm-2019-057

26. Rizzi A, Roy S, Bellenger JP, Beauregard PB. Iron Homeostasis in Bacillus subtilis Requires Siderophore Production and Biofilm Formation. Liu SJ, editor. Appl Environ Microbiol. 2019 Feb;85(3). Available from: https://journals.asm.org/doi/10.1128/AEM.02439-18

27. Propolsky D, Romanovski V. Iron and manganese removal from groundwater: comprehensive review of filter media performance and pathways to polyfunctional applications. Environ Sci Water Res Technol. 2025;11(11):2499–515. Available from: https://xlink.rsc.org/?DOI=D5EW00751H

28. Verma L, Ekka A, Banjara RA, Ambade B, Kumar A, Gautam S. A Review on Bacterial Exopolysaccharides for Heavy Metal Remediation: Mechanisms, Challenges, and Sustainable Applications. Water Environ Res. 2025 Oct 10;97(10). Available from: https://onlinelibrary.wiley.com/doi/10.1002/wer.70184

29. Strzelecki P, Nowicki D. Tools to study microbial iron homeostasis and oxidative stress: current techniques and methodological gaps. Front Mol Biosci. 2025 Jul 30;12. Available from: https://www.frontiersin.org/articles/10.3389/fmolb.2025.1628725/full

30. Li F, Cai J, Zhao X, Liu H, Ju F, Li Y. Research Progress in the Remediation of Arsenic- and Cadmium-Contaminated Groundwater Mediated by Iron and Manganese Biomineralization. Catalysts. 2025 Jun 9;15(6):570. Available from: https://www.mdpi.com/2073-4344/15/6/570

31. Shen L, Zhu X, Jiang H, Zhang J, Chen C, R. Reinfelder J, et al. Physical Contact between Bacteria and Carbonaceous Materials: The Key Switch Triggering Activated Carbon and Biochar to Promote Microbial Iron Reduction. Environ Sci Technol. 2025 May 20;59(19):9576–86. Available from: https://pubs.acs.org/doi/10.1021/acs.est.4c14024

32. Jhariya U, Chien MF, Umetsu M, Kamitakahara M. New insights into immobilized bacterial systems for removal of heavy metals from wastewater. Int J Environ Sci Technol. 2025 May 10;22(9):8319–34. Available from: https://link.springer.com/10.1007/s13762-025-06369-6

33. Patil A, Arya M, Yadav BK, Nahar M, Rajamohan N. Removal of toxic arsenic and chromium from soil using biochar-immobilized Geobacillus and Bacillus species: a review. Int J Environ Sci Technol. 2025

744 Nov 2;22(15):16143–66. Available from: https://link.springer.com/10.1007/s13762-025-06676-y

745 34. Mahajan A, Singhal P, Negi S, Kumar R, Jaswal VS, Ibrahim AA, et al. Microbial Strategies for the
746 Removal of Hexavalent Chromium from Wastewater: Recent Advances and Future Prospects. Water,
747 Air, Soil Pollut. 2025 Dec 4;236(14):894. Available from: https://link.springer.com/10.1007/s11270-
748 025-08522-w

749 35. Andrada Suarez EE, Roca Jalil ME, Fernandez Baldo MA, Cuozzo SA. Nanobiotechnology approaches
750 for the remediation of persistent and emerging organic pollutants: strategies, interactions, and
751 effectiveness. Environ Sci Nano. 2025;12(2):979–1011. Available from:
752 https://xlink.rsc.org/?DOI=D4EN00424H

753 36. Pal A, Bhattacharjee S, Saha J, Sarkar M, Mandal P. Bacterial survival strategies and responses under
754 heavy metal stress: a comprehensive overview. Crit Rev Microbiol. 2022 May 4;48(3):327–55.
755 Available from: https://www.tandfonline.com/doi/full/10.1080/1040841X.2021.1970512

756 37. Kayoumu M, Wang H, Duan G. Interactions between microbial extracellular polymeric substances and
757 biochar, and their potential applications: a review. Biochar. 2025 Mar 18;7(1):62. Available from:
758 https://link.springer.com/10.1007/s42773-025-00452-4

759 38. Najim AA, Radeef AY, Al-Doori I, Jabbar ZH. Immobilization: the promising technique to protect and
760 increase the efficiency of microorganisms to remove contaminants. J Chem Technol Biotechnol. 2024
761 Aug 29;99(8):1707–33. Available from:
762 https://scijournals.onlinelibrary.wiley.com/doi/10.1002/jctb.7638

763 39. Wang D, Root RA, Chorover J. Biochar-templated surface precipitation and inner-sphere complexation
764 effectively removes arsenic from acid mine drainage. Environ Sci Pollut Res. 2021 Sep
765 18;28(33):45519–33. Available from: https://link.springer.com/10.1007/s11356-021-13869-8

766 40. Hegazy GE, Soliman NA, Ossman ME, Abdel-Fattah YR, Moawad MN. Isotherm and kinetic studies of
767 cadmium biosorption and its adsorption behaviour in multi-metals solution using dead and immobilized
768 archaeal cells. Sci Rep. 2023 Feb 13;13(1):2550. Available from:
769 https://www.nature.com/articles/s41598-023-29456-5

770 41. Patel HK, Kalaria RK, More BS, Jokhakar PH, Khimani MR. Microbial ecology of biofiltration. In: An
771 Innovative Role of Biofiltration in Wastewater Treatment Plants (WWTPs). Elsevier; 2022. p. 235–66.
772 Available from: https://linkinghub.elsevier.com/retrieve/pii/B9780128239469000085

773 42. Alsawy T, Rashad E, El-Qelish M, Mohammed RH. A comprehensive review on the chemical
774 regeneration of biochar adsorbent for sustainable wastewater treatment. npj Clean Water. 2022 Jul
775 11;5(1):29. Available from: https://www.nature.com/articles/s41545-022-00172-3

776 43. Ajeng AA, Abdullah R, Ling TC. Biochar-Bacillus consortium for a sustainable agriculture:
777 physicochemical and soil stability analyses. Biochar. 2023 Mar 24;5(1):17. Available from:
778 https://link.springer.com/10.1007/s42773-023-00215-z

44. Schommer VA, Nazari MT, Melara F, Braun JCA, Rempel A, dos Santos LF, et al. Techniques and mechanisms of bacteria immobilization on biochar for further environmental and agricultural applications. Microbiol Res. 2024 Jan;278:127534. Available from: https://linkinghub.elsevier.com/retrieve/pii/S0944501323002367

45. Sharma V, Singh P, Trivedi B, Kamboj N, Bisht A, Pandey N. Assessment of Iron Biosorption Potential by Live and Dead Biomass of Bacillus subtilis (MN093305) from Aqueous Solution. Indian J Microbiol. 2024 Mar 18;64(1):153–64. Available from: https://link.springer.com/10.1007/s12088-023-01144-y

46. Kumari S, Kumar P, Kiran S, Kumari S, Singh A. Optimization of Siderophore Production by Bacillus subtilis DR2 and Its Effect on Growth Promotion of Coriandrum sativum. Russ Agric Sci. 2022 Dec 16;48(6):467–75. Available from: https://link.springer.com/10.3103/S1068367422060076

47. Bahuguna M, Joshi N, Bhandari G, Singh P, Gupta S, Rafatullah M, et al. Biological removal of iron content from water sources using iron-oxidizing bacteria: a review. Environ Pollut Bioavailab. 2025 Dec 31;37(1). Available from: https://www.tandfonline.com/doi/full/10.1080/26395940.2025.2556182

48. Hu W, Duan R, Dai Q, Yang H, Zhang Y, Meng F, et al. Effects of biochar immobilization Bacillus subtilis on heavy metal accumulation, rhizosphere microorganisms, and metabolism in rice. J Appl Microbiol. 2025 Apr 1;136(4). Available from: https://academic.oup.com/jambio/article/doi/10.1093/jambio/lxaf083/8105716

49. Huang J, Wang J, Wang S, Guo S. Different biochars as microbial immobilization substrates for efficient copper II removal. Spectrosc Lett. 2020 Oct 20;53(9):712–25. Available from: https://www.tandfonline.com/doi/full/10.1080/00387010.2020.1824196

50. Qi X, Gou J, Chen X, Xiao S, Ali I, Shang R, et al. Application of mixed bacteria-loaded biochar to enhance uranium and cadmium immobilization in a co-contaminated soil. J Hazard Mater. 2021 Jan;401:123823. Available from: https://linkinghub.elsevier.com/retrieve/pii/S0304389420318124

51. Bott KF, Wilson GA. Development of competence in the Bacillus subtilis transformation system. J Bacteriol. 1967;94(3):562–70. Available from: /doi/pdf/10.1128/jb.94.3.562-570.1967?download=true

52. Adebajo SO, Akintokun PO, Ojo AE, Akintokun AK, Badmos OA. Recovery of Biosurfactant Using Different Extraction Solvent by Rhizospheric Bacteria Isolated from Rice-husk and Poultry Waste Biochar Amended Soil. Egypt J Basic Appl Sci. 2020 Jan 1;7(1):252–66. Available from: https://www.tandfonline.com/doi/full/10.1080/2314808X.2020.1797377

53. Razzak A, Shafiquzzaman M, Haider H, Alresheedi M. Arsenic removal by iron-oxidizing bacteria in a fixed-bed coconut husk column: Experimental study and numerical modeling. Environ Pollut. 2021 Mar 1;272:115977.

54. Pundir S, Kandari V, Singh P, Singh R, Siddique MA. Assessment of groundwater quality of Dehradun Valley, Uttarakhand, India, for drinking purposes using multivariate statistical techniques. Environ Dev Sustain. 2022 Nov 21;26(1):1749–79. Available from: https://link.springer.com/10.1007/s10668-022-

02784-8

55. Aziz S, Uzair B, Ali MI, Anbreen S, Umber F, Khalid M, et al. Synthesis and characterization of nanobiochar from rice husk biochar for the removal of safranin and malachite green from water. Environ Res. 2023 Dec;238:116909. Available from: https://linkinghub.elsevier.com/retrieve/pii/S0013935123017139

56. Halder S, Wang Z, Roy PK, Sedighi M. Improving the adsorption properties of low surface area hardwood biochar for the removal of Fe+ and $PO_4 3-$ from aqueous solution. Environ Sci Pollut Res. 2024 Oct 13;31(51):60936–58. Available from: https://link.springer.com/10.1007/s11356-024-35249-8

57. Sema AI, Khatri J, Bijayi Dhar B, Kulsi G, Bhattacharyya J. On the Utility of Teakwood Biochar for Iron Contaminants Removal from Water. ES Mater Manuf. 2023; Available from: https://www.espublisher.com/journals/articledetails/871

58. Langmuir I. THE CONSTITUTION AND FUNDAMENTAL PROPERTIES OF SOLIDS AND LIQUIDS. PART I. SOLIDS. J Am Chem Soc. 1916 Nov 1;38(11):2221–95. Available from: https://pubs.acs.org/doi/abs/10.1021/ja02268a002

59. Freundlich H. Über die Adsorption in Lösungen. Zeitschrift für Phys Chemie. 1907 Oct 1;57U(1):385–470. Available from: https://www.degruyter.com/document/doi/10.1515/zpch-1907-5723/html

60. Promariya A, Mäenpää P, Incharoensakdi A, Raksajit W. Biosorption of iron(III) from aqueous solution by dried biomass of Synechocystis sp. PCC 6803. J Appl Phycol. 2021 Aug 1 [cited 2023 Mar 22];33(4):2313–25. Available from: https://link.springer.com/article/10.1007/s10811-021-02456-6

61. Redlich O, Peterson DL. A Useful Adsorption Isotherm. J Phys Chem. 1959 Jun 1;63(6):1024–1024. Available from: https://pubs.acs.org/doi/abs/10.1021/j150576a611

62. Abed EAM, Alaboudi KAN, Abbas MHH, Attia TMS, Abdelhafez AA. Iron Contamination in Groundwater: Risk Assessment and Remediation Techniques in Egypt's New Valley. Water. 2024 Jun 27;16(13):1834. Available from: https://www.mdpi.com/2073-4441/16/13/1834

63. Muhammad LH, Ibrahim MB. Biosorption of iron by heavy-metal tolerant *Micrococcus* sp. Bayero J Pure Appl Sci. 2018 Oct;11(1):102–9. Available from: https://www.ajol.info/index.php/bajopas/article/view/178443

64. Wang A, Dang Z, Wang Y, Fan H, Miao S. Efficient Inorganic Stabilization Materials for Chromium and Arsenic Pollution in Water and Soil. Appl Sci. 2025 Jun 23;15(13):7069. Available from: https://www.mdpi.com/2076-3417/15/13/7069

65. Zhu X, Wang K, Ma X, Zhang Z, Wang J, Zhang X, et al. Loading organic phosphorus-degrading bacteria enhanced biochar performance for heavy metals adsorption. Environ Technol Innov. 2024 May;34:103585. Available from: https://linkinghub.elsevier.com/retrieve/pii/S2352186424000610

66. Wang Z, Chen B, Cao Y, Xing S, Zhang B, Wang S, et al. Insights into the interfacial dynamics and interaction mechanisms between phosphate-solubilizing bacteria and straw-derived biochar. Biochar.

2025 Mar 13;7(1):55. Available from: https://link.springer.com/10.1007/s42773-025-00444-4

67. Ghosh S, Bhattacharya J, Nitnavare R, Webster TJ. Heavy Metal Removal by Bacillus for Sustainable Agriculture. In: Bacilli in Agrobiotechnology. 2022. p. 1–30. Available from: https://link.springer.com/10.1007/978-3-030-85465-2_1

68. Wang D, Chen H, Han H, Yang W, Sun Q, Cao C, et al. Interaction of biochar with extracellular polymers of resistant bacteria restrains Pb(II) adsorption onto their composite: Macro and micro scale investigations. Bioresour Technol. 2024 Dec;414:131602. Available from: https://linkinghub.elsevier.com/retrieve/pii/S0960852424013063

69. Rechberger M V., Kloss S, Wang SL, Lehmann J, Rennhofer H, Ottner F, et al. Enhanced Cu and Cd sorption after soil aging of woodchip-derived biochar: What were the driving factors? Chemosphere. 2019 Feb;216:463–71. Available from: https://linkinghub.elsevier.com/retrieve/pii/S0045653518319556

70. Madeira JP, Alpha-Bazin BM, Armengaud J, Duport C. Methionine Residues in Exoproteins and Their Recycling by Methionine Sulfoxide Reductase AB Serve as an Antioxidant Strategy in Bacillus cereus. Front Microbiol. 2017 Jul 26;8. Available from: http://journal.frontiersin.org/article/10.3389/fmicb.2017.01342/full

71. Syed Z, Sogani M, Rajvanshi J, Sonu K. Microbial Biofilms for Environmental Bioremediation of Heavy Metals: a Review. Appl Biochem Biotechnol. 2023 Sep 28;195(9):5693–711. Available from: https://link.springer.com/10.1007/s12010-022-04276-x

72. Wang Y, Chen L, Zhu Y, Fang W, Tan Y, He Z, et al. Research status, trends, and mechanisms of biochar adsorption for wastewater treatment: a scientometric review. Environ Sci Eur.. 2024 Feb 12;36(1):25. Available from: https://enveurope.springeropen.com/articles/10.1186/s12302-024-00859-z

73. Mei Y, Zhuang S, Wang J. Adsorption of heavy metals by biochar in aqueous solution: A review. Sci Total Environ. 2025 Mar;968:178898. Available from: https://linkinghub.elsevier.com/retrieve/pii/S0048969725005339

74. Li Z, Xiao X, Xu T, Chu S, Wang H, Jiang K. Removal of Pb(II) and Cd(II) from a Monometallic Contaminated Solution by Modified Biochar-Immobilized Bacterial Microspheres. Molecules. 2024 Oct 8;29(19):4757. Available from: https://www.mdpi.com/1420-3049/29/19/4757

75. Wang J, Guo X. Adsorption kinetics and isotherm models of heavy metals by various adsorbents: An overview. Crit Rev Environ Sci Technol. 2023 Nov 2;53(21):1837–65. Available from: https://www.tandfonline.com/doi/full/10.1080/10643389.2023.2221157

76. Chu KH, Hashim MA, Zawawi MH, Bollinger JC. The Weber–Morris model in water contaminant adsorption: Shattering long-standing misconceptions. J Environ Chem Eng. 2025 Aug;13(4):117266. Available from: https://linkinghub.elsevier.com/retrieve/pii/S2213343725019621

77. do Nascimento FH, Infante CMC, Pereira EAO, Leite ST, Masini JC. Empirical adsorption kinetics: comparing linear and nonlinear regression analysis emphasizing the need for high throughput analysis. J

Environ Sci Heal Part B. 2023 Jul 3;58(7):539–53. Available from: https://www.tandfonline.com/doi/full/10.1080/03601234.2023.2238591

78. Wu J, Wang T, Shi N, Pan WP. Insight into mass transfer mechanism and equilibrium modeling of heavy metals adsorption on hierarchically porous biochar. Sep Purif Technol. 2022 Apr;287:120558. Available from: https://linkinghub.elsevier.com/retrieve/pii/S1383586622001186

79. Da'ana DA, Zouari N, Ashfaq MY, Abu-Dieyeh M, Khraisheh M, Hijji YM, et al. Removal of Toxic Elements and Microbial Contaminants from Groundwater Using Low-Cost Treatment Options. Curr Pollut Reports. 2021;7(3):300–24.

80. De I, Tandel V. Social cost–benefit analysis of natural treatment systems in India: implications for benefits model and governance. Water Int. 2024;49(8):991–1011. Available from: https://doi.org/10.1080/02508060.2024.2431795